DELFT UNIVERISTY OF TECHNOLOGY
FACULTY OF CIVIL ENGINEERING AND GEOSCIENCES
DEPARTMENT OF HYDRAULIC ENGINEERING

HYDRAULIC RESPONSE OF A CREST WALL UNDER FOCUSED WAVE ATTACK

CIEM0120: RESEACH INTERNSHIP

MARIA SKLIA

TUDelft

Hydraulic response of a crest wall under focused wave attack

By

Maria Sklia

CIEM0120: Research Internship

in partial fulfilment of the requirements for the degree of

Master of Science

In Civil Engineering

at the Delft University of Technology,

Supervisor:	Dr. Ir. Bas Hofland,	TU Delft
Auxiliary Assessor:	Dr. Ir. Alessandro Antonini,	TU Delft

An electronic version of this report is available at http://repository.tudelft.nl

TU Delft

The reader is invited to commence this report by reading through the following abstract about waves, and sceneries somewhere in between the Netherlands, and Greece. I hope you enjoy reading this report as much as I enjoyed writing it.

Delft, August 2024

You're wrong, my dear friend, the boat is going at a good pace, but the Zuider Zee is a dead sea, or almost. With its flat shores, lost in the mist, one can't tell where it starts and where it ends. So, we're proceeding with no points of reference, and we can't assess our speed. We are going forward, but nothing changes; this is not sailing, but a dream. I had the opposite impression when I was in the Aegean, where new islands were constantly appearing on the rim of the horizon; night and day along the crests of the short, cool waves in a race full of foam and laughter."

La Chute (The Fall), Albert Camus (1956)

Abstract

Armoured slopes are commonly used in coastal structures to dissipate wave energy and protect adjacent infrastructure. To limit the height of these slopes in an efficient manner, regularly a concrete crest wall is placed at the upper part of the slope. Understanding the loads on these crest walls is essential for the design of coastal protection works. Conducting scaled physical model tests is a well-established approach to confirm and optimise the design of coastal structures, albeit time-consuming, scattered, and costly. This study aims to investigate the use of compact, focused wave signals in comparison to the common practice of using wave signals typically comprising a thousand waves in physical model tests. The physical model tests conducted in this study revealed that a compact wave signal was able to reproduce the extreme hydraulic response recorded during the simulation of a thousand irregular waves. This was observed in terms of sliding failure and extreme pressures exerted at the front vertical wall of the model crest wall. Results showed that the shape of the pressure signals, pressure distributions and integrated forces are reasonably well reproduced during focused waves. This suggests that this approach is promising for reproducing extreme responses at crest walls using focused waves; thus, resulting in reduced testing times. However, findings so far cannot support the use of this approach as a standalone tool for this application.

KEYWORDS: physical modelling, crest wall, focused wave, breakwater, impact pressures

Table of Contents

1. Introduction

1.1 Breakwater design

Harbours are bound to societies and their evolution since ancient times, as port cities were hubs of commerce and culture. As such, the design and construction of ports is one of the most ancient branches of engineering - with evidence that rubble mound breakwaters with length of a few kilometres existed in the mediterranean region about 2000 BC (Wiegel, 1964). Several approaches with respect to materials were made, with Egyptians opting for cyclopic dry stone, Greeks using ashlar masonry held together by iron dowels and lead, while Romans built with concrete, in a mixture including pozzolanic ash, lime and stone (Saville, 1940). Saville mentions the characteristic geometry of arcade breakwaters (Figure 1.1) already present in ancient times, built in an attempt to deal with silting in the entrance of the harbour, with the characteristic example of the ancient port of Ostia in Italy, known as Civita Vecchia, in modern times. It has been established that efficient design of coastal structures is not a new problem. On the contrary, the economic design of coastal structures is a problem, yet to be completely solved, involving the complex interaction of waves and structures (Hughes, 1979, after Hughes 1993).

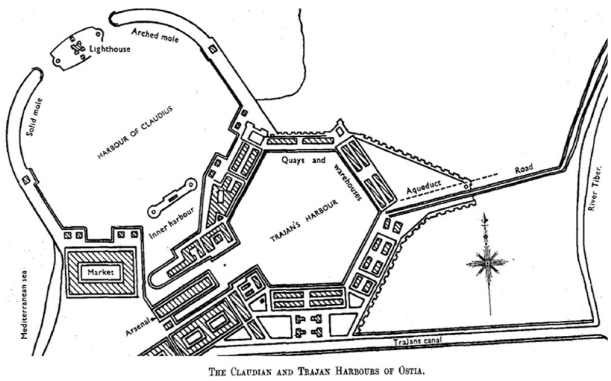

THE CLAUDIAN AND TRAJAN HARBOURS OF OSTIA.

(a)

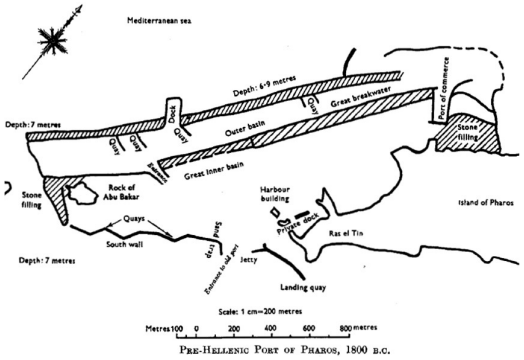

PRE-HELLENIC PORT OF PHAROS, 1800 B.C.

(b)

(c)

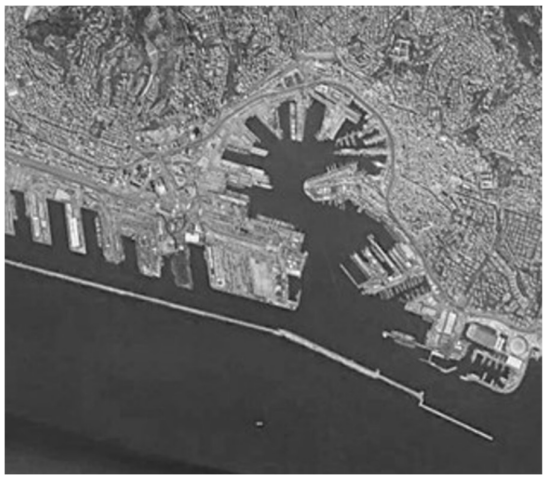

(d)

Figure 1.1 Historical Breakwater layouts. (a): Port of Ostia, Rome, c. 40 AD Seville (1940), (b): port of Pharos (then Alexandria) c. 1400 BC (Seville, 1940), (c): Port of IJmuiden, Netherlands 1980, (d): Genoa port, Italy 2020.

Several parameters are involved in the successful design of a breakwater, in essence to prevent the three major failure mechanisms, i.e., sliding, overturning and geotechnical failure of the foundation. Goda (2000), in his book Random Seas and Design of Maritime Structures, summarises two broad requirements for the design of breakwaters. First, the main structural elements should be strong enough to withstand the storm waves, and second; the crest elevation should be high enough to prevent large volumes of water from reaching the lee side of the structure. The first requirement can be translated into the wave induced forces acting upon the coastal structure, which are traditionally measured in physical model tests via pressure gauges, and sliding failure that can be recorded in terms of horizontal displacement. The second requirement relates to wave overtopping, the study of which is outside the scope of this project.

Goda (2000) draws the attention of the reader to the care that must be taken regarding the impulsive wave pressures at vertical breakwaters. Such pressures can be created for instance when the forward momentum of a wave front is converted into an impulse exerted on the seaward vertical face of the coastal structure, essentially when the wave breaks in the vicinity of the vertical wall and collides with it. Systematic investigations of wave impact forces on the vertical elements of coastal structures are carried out for more than sixty years in model flumes e.g., Lungren (1969), with studies published before the war still being highly relevant (i.e., Bagnold in 1939). Bagnold investigated the physics of the wave impact on a vertical wall in a laboratory flume with glass walls, steered solitary waves and made significant observations regarding the conditions under which a wave impact occurs. Issues regarding the presence of air in the formation of different wave impact types, the magnitude and nature of impact pressures, together with the inaccuracy of scaling up model results of impact pressures are already recognised by the scientific community and discussed in the proceedings of "Research on wave action" symposium organised by Delft Hydraulics Laboratory in 1969. Research is still ongoing in this field today, as many aspects of this type of wave-structure interaction are yet to be fully understood.

There is still room for research in the physics of wave breaking and wave impact on coastal structures, and a constant need to provide accurate and up-to-date design guidelines regarding the vertical and uplift pressures exerted on coastal structures. The latter becomes particularly relevant in breakwaters with emerged crest walls. This type of structure is modelled to scale in a laboratory flume in this study. Determining the pressure distribution on the vertical and horizontal face of a crest wall is essential for the design and has been subject to several theories through the years regarding the pressure distribution specifically in vertical coastal defences, such as seawalls, incorporating rubble mound foundation. Relevant to the refining of existing design guidelines which more often than not originate from physical model tests, Hughes (1993) mentions "optimising a structure often can only be achieved by systematic physical model tests".

In order to model the hydraulic response of any coastal structure in a laboratory flume, a set of boundary conditions need to be specified for the wave forcing. The waves in hydraulic engineering labs focusing on modelling coastal structures are typically generated by piston type wave makers which can reproduce a signal of irregular timeseries representative of a storm, or the so-called design sea state. Standard practise dictates the simulation of a thousand waves in physical model tests, which corresponds roughly to testing times around half an hour per test for the modelling of one testing condition. Several studies have been made in the last 20 to 30 years offering an alternative solution for the applied wave boundary conditions in physical model tests, that is by using a compact, focused wave signal, that would represent the maximum wave height of the design sea state, essentially generating the extreme conditions leading to significant time savings of test durations. This type of wave forcing is not limited per application, as it can be used to model for example extreme wave overtopping or run up, maximum pressure signals or forces during wave impacts.

1.2 Scope

The scope of this study is to identify if a focused wave signal can sufficiently reproduce an extreme hydraulic response of a crest wall in comparison to the wave forcing by an irregular sea state comprising one thousand waves. In order to achieve this, a custom signal is prescribed at the paddle so that the waves can focus and obtain the

maximum wave height in the flume, with that maximum wave height, focus location and free surface surrounding the wave crest at focus being predefined. In that sense, the possibility of using compact focused wave signals to reproduce extreme responses can be assessed.

1.3 Objectives

To investigate wave impacts and the associated extreme hydraulic responses at crest walls by forcing a focused, compact wave signal the following objectives are formulated:

1. Prepare and model in a physical wave flume a focused wave signal.
2. Generate a focused wave impact at a crest wall placed on top of a rubble mound breakwater and assess the extreme hydraulic response in terms of the recorded pressure signals and sliding failure.
3. Compare the recorded response of the crest wall during the focused wave test (as described in the second objective) to the extreme hydraulic response recorded during an irregular wave series comprising one thousand waves in terms of the recorded pressure signals, pressure distributions and impact forces.

1.4 Approach

The first objective is fulfilled by prescribing a custom steering file at the wave machine. This wave signal is prescribed to focus at predefined locations along the flume and the structure to reach a target extreme wave height that corresponds to certain extreme exceedance percentages in the Rayleigh distribution of a random sea state, e.g., $H_{0.1\%}$ and $H_{0.01\%}$. The second objective is pursued by calibrating the focused wave signals in the wave flume so that focusing occurs in the vicinity of the structure. Following, the wave impact is assessed by analysing the recorded pressure signals and displacements that occurred during the focused wave simulations. The third objective is accomplished by comparing the hydraulic response of the crest wall during the irregular wave tests and the focused wave tests by means of comparing the following: i) the wave impact pressures for the ensemble of pressure gauges placed on the front wall and the horizontal face of the crest wall. ii) the pressure distributions on the vertical wall and the horizontal face of the crest wall. iii) the integrated forces on the model crest wall.

1.5 Outline

The report is structured as follows:

Chapter 1 serves an introduction to breakwater design over the past centuries and provides the motivation and context of breakwater design in recent years, and last, the outline of the report is presented.

Chapter 2 provides the theoretical background into modelling irregular waves, and wave-structure interaction. Specifically, formulations that describe a random sea state are presented along with the theory necessary to generate waves in laboratory flumes, basic information about testing coastal structures in a physical model and previous studies on impulsive loads on coastal structures.

Chapter 3 describes the methodology used in this study regarding the formulation of the focused wave signal, the experimental setup in the flume, the testing process and test programme.

Chapter 4 summarises the main findings of this study that originate from the physical model tests organised in three subchapters. First, the focused wave signals recorded in the wave flume are presented. Following, the hydraulic response of the crest wall is assessed when subject to focused wave attack, in terms of recorded pressures, and sliding failure. In the third, and last, section of chapter four the recorded pressure signals are illustrated as pressure signals, integrated forces, and pressure distributions for both the focused waves and irregular waves and results of this comparison are discussed.

Chapter 5 summarises key observations on the comparison of extreme hydraulic response of crest walls placed on top of rubble mounds under focused wave attack. Following, conclusions are drawn with respect to the comparison of the hydraulic response accounting for irregular wave tests and recommendations are given for future research.

2. Theoretical Background

2.1. Modelling waves

2.1.1. Description of Random Seas

Designing coastal structures is bound to carefully determining wave loads acting on the structure. In the case of open seas, where wind generated waves are the dominant forcing mechanism, the so-called design sea state must be determined, which is often associated to a storm with characteristics linked to a particular area, for instance, water depth, bathymetry, coastline orientation, fetch length and native wind conditions. To avoid describing the sea state in a deterministic way, using single values of wave height and wave period, the concept of energy spectrum is used, so that the sea state can be described as a stochastic process. In that way, an observation is just one realization of the stochastic process. The random-phase amplitude model is then introduced to reconstruct a sea state. According to this model formulation, any sea state can be reproduced by summing up a sufficiently large number of harmonic wave components. If a fixed point in space is set, for instance a buoy, then the wave signal can be described as follows (Goda, 2000):

$$\eta = \eta(x, y, t) = \sum_{n=1}^{\infty} a_n \cos(k_n x \cos\theta_n + k_n y \sin\theta_n - 2\pi f_n t + \varphi_n) \qquad \textit{Equation 1}$$

For each frequency, f_n, the values of amplitude, a_n and phase, φ_n can be prescribed by using Fourier series and derive the amplitude and phase spectrum, respectively. The phase, φ, is assumed to be randomly and uniformly distributed, while the amplitude is assumed to follow the Rayleigh distribution. To add wave directionality in Equation 1 so that waves of different frequencies that propagate towards different directions are accounted for, the following formulation is relevant.

In the formulation of Equation 2, k is the wave number, $k = 2\pi / \lambda$, θ is the angle of incidence, and φ the phase.

The next step of application of the random phase amplitude model is in the definition of the wave spectrum. This is achieved by calculating the summation of the squared wave amplitudes over a frequency interval.

$$\sum_{n}^{f+df} (\tfrac{1}{2} a_n^2) = S(f)df \qquad \textit{Equation 2}$$

In nature, as the wave field is three-dimensional, wave direction is also included in the spectrum, and becomes relevant in terms of the dominant wave direction and the associated directional spreading.

The formulation of equation 2 can also be mathematically derived following the principle of representing a random sea state as a stochastic process by applying three fundamental assumptions about the free surface elevation of the sea, i.e., stationarity, ergodicity and gaussian distribution of the wave amplitudes. In this case the spectrum is expressed in terms of the autocovariance function of the sea state (Goda, 2000), i.e.,

$$\mathrm{E}[\eta(t+\tau)\eta(\tau)] = \mathrm{E}[\eta(\tau)\eta(0)] \equiv \psi(\tau) \qquad \textit{Equation 3}$$

Here, the stationarity condition is applied to the autocovariance function. Then the autocovariance function is formulated as follows: $\psi(\tau) = \int_0^{\infty} S(f)\cos(2\pi f)\tau df$ and can be expressed in terms of the function S(f), as

$S(f) = 4\int_0^\infty \psi(\tau)\cos(2\pi f)\tau d\tau$, which after derivations, leads to $S(f) = \frac{1}{\Delta f}\sum_{n=1}^{f+\Delta f} \frac{1}{2}a_n^2$, which is in agreement with Equation 3. Note that the autocovariance function for τ=0, gives the variance of the wave profile, m_0.

$$m_o = \overline{\eta^2} = \int_0^\infty S(f)df = \psi(0) \qquad \textit{Equation 4}$$

The assumptions of stationarity, ergodicity and gaussian distribution must be used with care, as it is known that a sea state can be characterised by wind-induced wave growth, decay or dissipation, tidal variations etc., which directly make the assumptions of stationarity invalid. What is more, despite the fact the wave records seem to fit reasonably well to the Rayleigh distribution and that is considered common practice in coastal engineering practical applications; it has been found that extreme wave heights in shallow waters do not fit well this distribution, and the use of this distribution leads to an overestimate of wave heights. For more information about these matters, the reader is referred to, Holthuijsen (1999), Goda (2000),

For dispersive waves, which propagate in intermediate water depths the wavelength depends on water depth. This dependency is described by the dispersion relation, as follows:

$$\omega^2 = gk\tanh(kd) \qquad \textit{Equation 5}$$

Where, d: water depth, k: wave number, ω: wave angular frequency, g: gravitational acceleration

By substituting in equation 4 the definitions of the fundamental terms of wave number, k, and angular frequency, ω, the dispersion relation can be solved iteratively to obtain the wavelength for a specific depth, d, in the so-called intermediate depth regimes, typically relevant for the waves generated educational laboratory flumes.

The Rayleigh distribution was originally derived for the description of narrow banded sound waves with varying amplitudes. However, it is broadly used within the context of coastal engineering over many decades. It is established that wave heights from records of irregular ocean waves fit well in a Rayleigh distribution (Goda 2000, after Longuet Higgins 1952). According to the Rayleigh distribution, the maximum wave height of a wave record of N waves, is given by the following formulation.

$$H_{\max} = H_{rms}\sqrt{\ln N} = H_s\sqrt{\frac{1}{2}\ln N} \qquad \textit{Equation 6}$$

Where, H_{max}: the maximum wave height in a wave signal, H_s: the significant wave height (average of the upper one third of the wave record), N: the number of waves in the wave signal. Thereby the empirical relations of the maximum waves within a record, being $H_{max} \cong 1.86$ Hs, for N=1000 waves and $H_{max} \cong 2.15$ H_s, for N=10000 waves. A thorough description of the Rayleigh distribution is outside the scope of this work, the reader is therefore redirected to Waves in Oceanic and Coastal Waters, Holthuijsen (2007).

2.1.2. Wave steering in laboratory flumes

Steering waves in the laboratory flumes is an established way to simulate the hydraulic response of coastal structures. Biésel and Suquet (1954) formulated an equation for wave steering by piston type wave generators. The stoke of a piston type wave maker is given by the following equation:

$$\frac{H}{S_o} = \frac{4\sinh^2(kd)}{\sinh(kd)+2kd} \qquad \textit{Equation 7}$$

Where, H: free surface elevation, S_o: stroke (horizontal displacement) of the wave maker, d: depth, and k: wave number.

It has been observed that in piston type wave makers, one of the first and one of the last waves of the wave signal are significantly larger than the average. This phenomenon is attributed to the transient starting and stopping times of the wave paddle. This observation has been linked to the fact that the wave board, which in this case is a piston-type wave maker, does not exactly fit the walls and the bottom of the flume; this is commonly referred to as the phenomenon of leakage. Madsen studied this phenomenon in the 1970s and made experiments to quantify this observation. His findings are compared to experiments from Ursell in the 1960s and are presented in Madsen (1970). Specifically, it is stated that the area of the gaps around the piston of the flume was 2.7% of the wetted area and it was found that the leakage through the gaps reduced the wave height by 15%. It is also mentioned that the first large waves associated to the start of the wavemaker can be eliminated by tapering (fading in) the signal so that the stroke gradually reaches its maximum. In addition, if the wave board satisfies the boundary condition up to first order, then second order spurious waves will naturally form and inevitably pollute the experiment (Hughes 1993). Madsen formulated an approximate wavemaker theory that could suppress the free secondary wave. This formulation includes a second term in the wave board displacement, so that the second order harmonic is suppressed. First order wave theory is still broadly used, as its simplicity, ease of application in practice and acceptable accuracy for many applications seems to outweigh its shortcomings. Besides, as Madsen, 1970, points out, when focusing on the wave height, rather than the amplitude, the linear solution should cover at least the slightly nonlinear waves. More recently Mortimer et al. (2022) demonstrated the implications of second order wave generation, finding that sub-harmonic spurious waves are particularly important in shallow waters, as they result in overestimating run-up and dynamic forces. The background of this, also highly relevant to the present work: Free spurious waves compensate for the mismatch between water-wave kinematics and first-order steering. The sub-harmonic waves travel faster than the first-order wave group, thus the sub-harmonic spurious waves arrive at the testing section prior to the first order, and the second-order super-harmonic waves (Mortimer et al. 2022), interfering with the experiment, whereas the super-harmonic spurious waves travel slower, thus are not of major concern.

Handling reflections in wave flumes and wave basins is a matter of discussion in every physical modelling study. This issue is a phenomenon generated due to the closed boundaries of a flume or basin, while in nature a reflected wave would simply propagate in the open sea, whereas in a wave flume the reflected wave will reach the other side of the flume, where the wave paddle is located and then re-reflect on the vertical board. Therefore, a new parasitic wave remains in the paddle and alters the target wave field. This phenomenon gathers significant attention because the quality of the experiments is determined be the accuracy of the generated wave field, especially close to the structure, compared to the target wave field and, in order to improve this accuracy, reflections inside the paddle have to be minimised. In state-of-the-art laboratory facilities, wave generator systems with active reflection compensation are used, so that the displacement of the wave board accounts for the incoming wave heights, when generating the waves. For applications of modelling short wave signals, e.g. 1-2 minutes, the duration of the signal is shorter than the time needed for the waves to re-reflect and reach the structure, so ARC is less relevant.

2.1.3. Generation of extreme hydraulic responses via compact wave signals

Tromans et al. (1991) formulated an equation based on the random-phase amplitude model of Equation 2, and the amplitude following Equation 3, providing the most probable shape of the surface elevation shape (Figure 2.1) of an extreme, deterministic, wave, and tested it for loading of offshore structures, as an alternative to simulating time consuming, random sea states. This wave model is formulated as follows, in terms of the free surface elevation.

$$\eta^* = \eta_d^* + g(\tau) \quad or \quad \eta^* = a\psi(\tau) + g(\tau) \qquad \textit{Equation 8}$$

Where, α is the crest elevation, $\psi(\tau)$ is the autocorrelation function of the sea surface elevation. The first term in Equation 10 is the most probable, deterministic value, and it increases proportionally with the crest elevation. The second term on the right-hand side of equation 10, is a non-stationary gaussian process, with zero mean at the wave crest, and a standard deviation equal to the one of the wave fields at a certain distance from the crest. Hence, at the crest, the first term is dominant, and reads the following formulation:

$$\eta_d^* = a\sum_{i=1}^{N}\frac{S(\omega_i)}{\sigma^2}\Delta\omega\cos[k(x-x_f)-\omega_i(t-t_f)] \qquad \textit{Equation 9}$$

The variance of the sea state:

$$\sigma^2 = \sum S_{nn}(\omega_i)\Delta\omega = m_0 \qquad \textit{Equation 10}$$

The maximum wave amplitude of an irregular sea state by the Rayleigh distribution:

$$a = \sqrt{2m_0 \ln N} \qquad \textit{Equation 11}$$

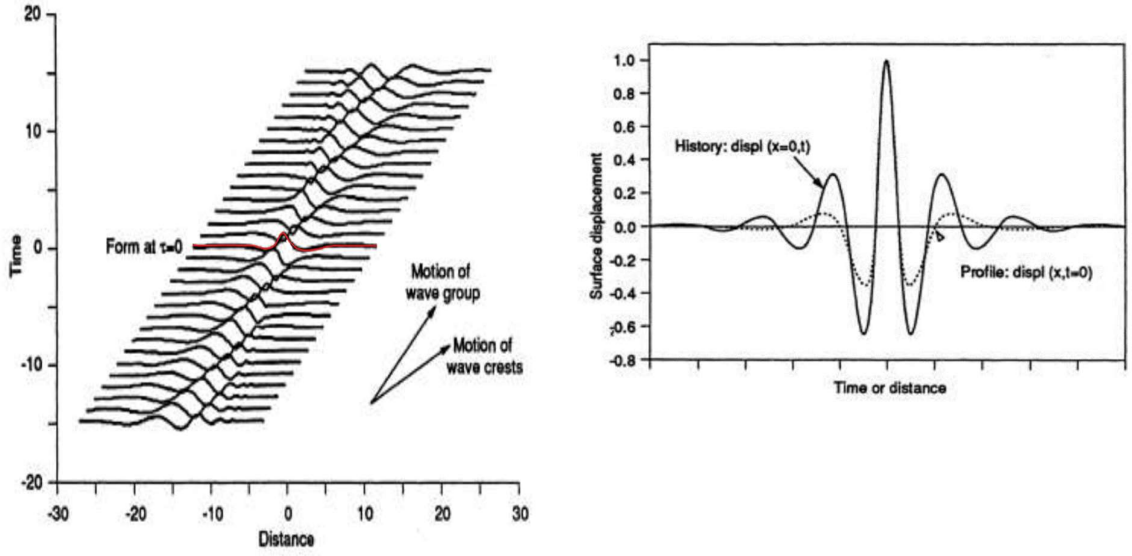

(a) (b)

Figure 2.1 Free surface elevation of focused waves. (a): Evolution of the focused wave signal in time and space (red line indicates the shape of the free surface at focus), b): Most probable free surface elevation for a PM Spectrum. Tromans et al. 1991.

Whittaker et al. 2016 optimised focused waves via a parametric study of 480 tests to investigate extreme runup events on a planar beach while applying both numerical and physical modelling. Second order steering was used to accurately reproduce the coastal response that is susceptible to transient waves that would otherwise contaminate the experiment. The parametric study revealed that wave amplitude at focus, focal distance from the wave maker, and the phase of the wave group at focus (that is for example: crest or trough focused group) were all important to determine the maximum runup. Whittaker mentions that since the amplitude at focus can be associated to a certain probability of occurrence, a runup event driven by such a wave can be simulated, so that it can be classified for example as the runup caused by the highest wave in a storm of N waves. It is also stated that the remaining subharmonic error that was not possible to be suppressed by the wavemaker, led to an onshore focal shift. Results showed that there are certain combinations of wave focal points and amplitudes at focus that can lead to maximum runup. The possibility of saturation while increasing the wave amplitude is commented, as it was noticed that the non-dimensional runup decreased for a certain increase of wave amplitude at focus, thus implying energy dissipation due to breaking. The focus location was used in this study to control the properties of the wave group rather than impose a specific target focal location. The author concludes that this approach can provide an efficient alternative to lengthy simulations to reproduce extreme hydraulic responses in coastal structures and act complementary to empirical formulae for runup estimates.

In the study of 2018, Whittaker et al. applied focused wave groups on a plane beach preceding a dike and modelled the hydraulic response in terms of wave overtopping and horizontal pressures on the dike geometry. The study revealed the importance of the preceding wave, that is, the occurrence of minimal reflection, in order to produce maximum overtopping and horizontal forces on the wall configuration. Furthermore, it is noted that maximum overtopping does not occur under the same parameter space of focused wave (location and phase) to the max horizontal forcing. Specifically, maximum horizontal forces were found to occur for focus locations inshore of the structure. It was found that for a given focal point and amplitude, tuning the group phasing can lead up to an order of magnitude difference in the total overtopping volume of the group. It is important to note, that due to the geometry of the foreshore ahead of the dike configuration, mainly pulsating loads were recorded.

Hofland et al. (2014) investigated the applicability of using compact wave signals to reproduce extreme overtopping events, so that long test durations can be reduced. Two approaches were used; first, a short-duration wave signal was sampled from an irregular sea state, and second, a focused wave signal was created according to the formulation of Tromans et al. (1991). In the implementation, focusing of phases was achieved via applying a correction of 5% to all phase velocities, which resulted in a more symmetric peak of the wave shape at focus. The rationale behind this experiment is that if wave height is the main parameter of influence in the wave overtopping process, generating a compact signal with a wave height corresponding to certain probability of exceedance from the irregular sea state, and a realistic shape of the free surface elevation, should reproduce an overtopping event of the same magnitude. Results showed that by applying the formulation of Tromans, overtopping volumes could be reproduced within a factor of 2, compared to testing an irregular sea state of a thousand waves, reaching the conclusion that it is possible to obtain an estimate of the individual overtopping volumes from testing a short, focused wave signal from a substitute sea state, compared to the design sea state of the thousand random waves.

Hofland et al. (2010) formulated a focused wave signal to specifically prescribe the position, and type, of wave breaking to generate wave impacts at a vertical wall in large scale experiments (Figure 2.2), within the context of investigating wave sloshing and forces acting upon the walls of LNG container tanks. Wave breaking types were classified as: aerated impact, air pocket impact, flip through and slosh impact. The first two differ relative to the amount and size of air pocket trapped between the broken wave and the vertical wall. The flip through impact indicates that crest and trough coincide in the vertical axis while impacting the wall, but the air is ejected upwards just before the impact. The sloshing impact is essentially the running up of a crest on the preceding wave, so it describes the superimposition of two crests, while the first is in contact with the wall. Results showed that air pocket and flip-through impacts produce the larger impact forces, while the latter generated significantly larger impact pressures.

Figure 2.2 Large scale wave impacts at vertical walls in the Delta flume, Deltares, Hofland et al. 2010. Left panel: Lee side of vertical wall, Mid panels: Wave propagation and breaking, Right panel: Wave impact at the vertical wall.

Altomare et al (2024, a) published preliminary results of a study on overtopping flow velocities in promenades with focused wave forcing, following the Tromans formulation. In this study, a non-intrusive measurement technique was used, i.e., bubble image velocimetry, to record the flow patterns and velocities. The aim of this study was to inform

the design of coastal promenades with emergent toes in highly urbanised coastal fronts that are susceptible to severe overtopping events. In this study, the advantages of using a compact wave signal related to repeatability of tests and time efficiency in testing extreme events are highlighted.

In the study of Altomare et al. (2024, b), focused wave groups are forced, following the Tromans' formulation, this time to study wave impacts on piers (Figure 2.3). This study is motivated by a structural failure of a pier during storm conditions in Spain. Numerical modelling and large-scale physical model tests were performed to study the fluid-structure interaction; with tested wave heights up to 1.11 m at focus. Wave climate projections for 2100 were accounted for in terms of sea level rise using the IPCC's RCP8.5 scenario. With respect to the phasing of wave groups and the importance of wave succession, this study revealed that for target trough-focused waves, the first incoming crest generated the maximum uplift force, while the second crest led to the max horizontal loading. It is noted that this succession could occur in a real sea state when two waves with high crests propagate within the same group and form a deep intervening trough. Comparisons of force distributions were made between the irregular sea state and focused waves, where horizontal forces displayed a higher proximity to the random sea state. A comparison of the forces from instances of similar hydrodynamic characteristics in the focused and irregular wave tests implied that forces induced by focused waves were relatively lower to the ones created in the random sea state. However, it is shown that the extended dataset of peak forces recorded during focused wave tests was able to cover a broad part of the distribution of maximum forces recorded during the simulation of the irregular wave trains.

Figure 2.3 **Left panel: Wave attack at pier, at Pont del Petroli during storm Gloria, source: Badalona City Council, Spain, Middle and Right panel: physical model tests at CIEM flume, at UPC, Spain, Altomare et al (2024, b).**

2.2. Physical modelling of coastal structures

Physical modelling in the context of coastal structures is a way to simulate natural processes, and their interaction with man-made structures in a controlled environment, so that the underlying physical mechanisms are understood, and the most relevant variables to the phenomena at hand are quantified. The following contradiction emerges in the laboratory models: they inherently reproduce the physical process without simplifying assumptions that typically appear in numerical modelling, however, the full-scale problem, in this case the wave-structure interaction has to be represented with some simplification, which is for example, a model breakwater. The most important notion that an engineer should keep in mind when designing a coastal structure model in the lab is that he has to ensure that the scale selection is appropriate for the phenomenon that is studied so that the dominant forces are well represented (Users guide to physical modelling and experimentation, 2011).

One of the drawbacks of physical model tests are the so-called scale-effects. Scale effects refer to the phenomena that appear in laboratory experiments and would not occur in the full scale of the problem. Here, also the type of testing facility becomes relevant. The presence of scale effects can lead to incorrect conclusions about the hydraulic response of the structure if the relevant physical mechanisms are not accurately represented. Sources of these scale effects are among others, the presence of air in highly aerated flows that appears for example in wave breaking, viscous scale effects, that appear for example in the core of modelled breakwaters,

and the different density in salty and mineral water. Typically, when there is evidence that scale effects appear and play a significant role in an experiment, the structure is tested on a larger scale in order to assess the importance of the scale effects and test the structure in more realistic dimensions.

Measurements of static or dynamic pressures become relevant in modelling coastal structures in case of waves impacting a vertical wall or if pore pressures inside a breakwater need to be measured. Measurements of dynamic pressures is achieved via commercially available pressure transducers. This type of pressure gauge is providing time history of the recorded pressures to capture the shape of the impulsive loading (Hughes 1993). More recent studies suggest that pressure records do not necessarily need to be sampled with a very high frequency acquisition to sufficiently describe wave-induced loads, as the magnitude of wave impulse can sufficiently describe the impulsive loads at vertical walls (Chen et al. 2014). Regarding the scaling of pressures, the following must be kept in mind: "Measured forces and pressures in Froude scaled models will be in similitude with the prototype equivalents, provided that the model does not experience any impact or impulsive loading from waves breaking directly on the structure" (Hughes, 1993).

Three types of breaking wave shapes impacting vertical walls are identified according to Lundgren (1969), that is: ventilated shock, compression shock, and hammer shock (Figure 2.4). These types of impacts can produce shock pressures of higher intensity compared to similar magnitude non-breaking waves. In these types of shocks there is always some air entrainment in the waveform that hits the wall. However, the shape of the waveform and the presence of air between the water volume and the impermeable obstacle (here a sea wall) differs. In the first type of impact, i.e., ventilated shock (or flip-through), the air escapes upwards, minimising air entrapment. As in this case the main forces are inertial and gravitational, Froude scaling applies, and impulses can be scaled to prototype. During a compression shock the air pocket trapped between the structure and the water mass is compressed during the impact. Since the air is not scaled according to Froude's law and in this case also surface tension becomes important, results from physical model tests encountering these types of impacts, it is not straightforward to directly scale up to prototype, especially when the dimensions of the air pocket are not known or measured.

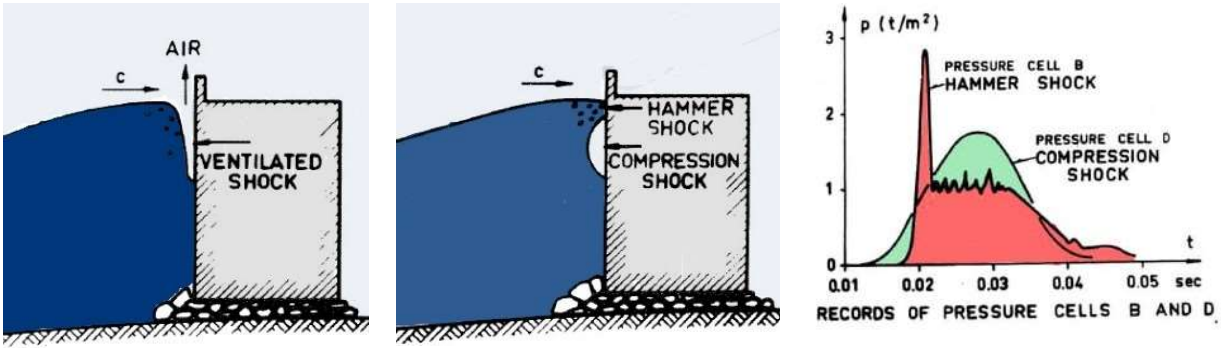

(a) (b) (c)

Figure 2.4 Types of wave impacts relative to air entrainment at vertical breakwaters. (a): Ventilated (or flip-through impact). (b): Combination of a hammer shock and compression shock. (c): pressure records for hammer shock and compression shock/ Adapted from Lundgren (1969).

Jensen's monograph on breakwaters (1984) gives a broad, yet thorough overview into the design of breakwaters. In that manuscript the reasoning behind placing crest walls as superstructure is mentioned, i.e., to reduce the crest elevation, to control overtopping flows or to provide further sheltering for adjacent infrastructure. Jensen (1984) also records that, in general, stability decreases for decreasing wave steepness. Relative to the wave induced forces, Jensen (1984) states that forces are a function of the velocity of the water impacting the structure, and its volume, with the water level, roughness of the armour, geometry and armour slope being the main parameters involved (see Figure 2.5, left panel). The time lag in the appearance of peak pressures in the horizontal and vertical face of the crest wall was also addressed in that manuscript. Regarding the pressure measurements it is mentioned that the sharp pressure peaks are attributed to the compression on air pockets and air bubbles, which are not reproduced to scale in the physical

model tests. With respect to the forces acting on the base of the crest wall, it is mentioned that these are forces due to pressures in compressible media, i.e. a mixture of water and air. The complex physics at an emerged crest wall, where the base level or foundation of the wall lies above the still water level was also addressed. The geometry dictates that the area of the porous core of the breakwater below the crest wall is normally filled with air. During wave forcing this air pocket is trapped and pushed to the leeside during the wave uprush in the armour layer, stating: "this phenomenon of squeezing out the air under the superstructure appears to cause oscillating pressures in the air trapped here". It is assumed that these peaks (Figure 2.5, right panel) occur due to air pockets and compression model law is used to convert them to a smooth pressure timeseries so that Froude scaling can be applied. Lastly, Froude's law can be applied to a well-ventilated shock but yields conservative results if bubble content in prototype is high and pressure rise times are short.

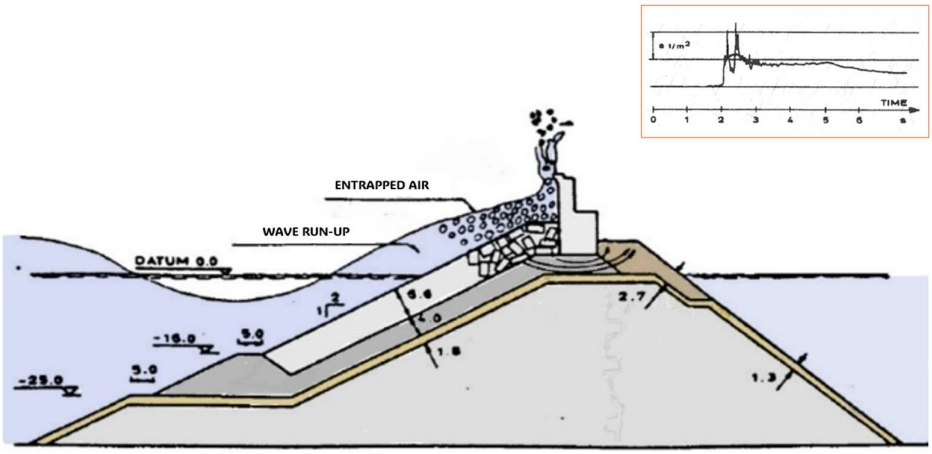

Figure 2.5 Example breakwater geometry and pressure record measured under the crest wall. Adapted from Jensen (1984).

Allsop's report (Allsop et al. 1996) on wave forces on vertical and composite breakwaters identified certain characteristic shapes of wave impacts and classified them in four different types, namely: impact pressure with short rise time, less severe impact or up-lift pressure at the time of the impact, double peaked pressures with longer rise times, and pulsating pressures. Following, in the same report, various distributions of uplift pressures are identified depending on the geometry of mound, water level with respect to the base plate of the crest wall and possible siltation on the lee side of the breakwater (i.e. the harbour basin). The latter could result in a rectangular pressure distribution (Allsop 1996, after Franco 1994) as the pressures cannot be released on the leeside of the porous core of the breakwater.

Pedersen (1996) performed more than 350 tests of random sea states to investigate fluid-structure interaction properties and stability in rubble mounds with crest walls. Three tested configurations are shown in Figure 2.6, include one fully sheltered front face of the crest wall by the armour layer, and two partially exposed crest walls, in which the front face of the crest wall is partly exposed to wave forces. Pedersen (1996) observed that the pressure rising times differ for these configurations. Specifically, rising times for the partly exposed crest walls (which are also more relevant to the present study), were found to be in the range of $\Delta t = 0.01 - 0.1$ s. Also, it can be seen from the pressure distribution over the vertical face of the crest wall, that for the most exposed configuration, the peak pressure occurs somewhat above the geometrical centre of the wall over the vertical axis. Pedersen highlights that crown walls with an upper unprotected part are subject to high impact pressures. Pedersen also noticed that for the higher wall the majority of the tests displayed a single pressure peak, where rise, decay and quasi-static part are easy to distinguish (Bagnold 1939). Pedersen concluded that for the highest crest wall configuration, half exposed to wave loads, the pressure distribution displays the peak pressure just above the armour layer and this occurs consistently for waves that break on the armour slope. Note that pressures were recorded with acquisition frequency about 250 Hz for the two exposed crest wall configurations.

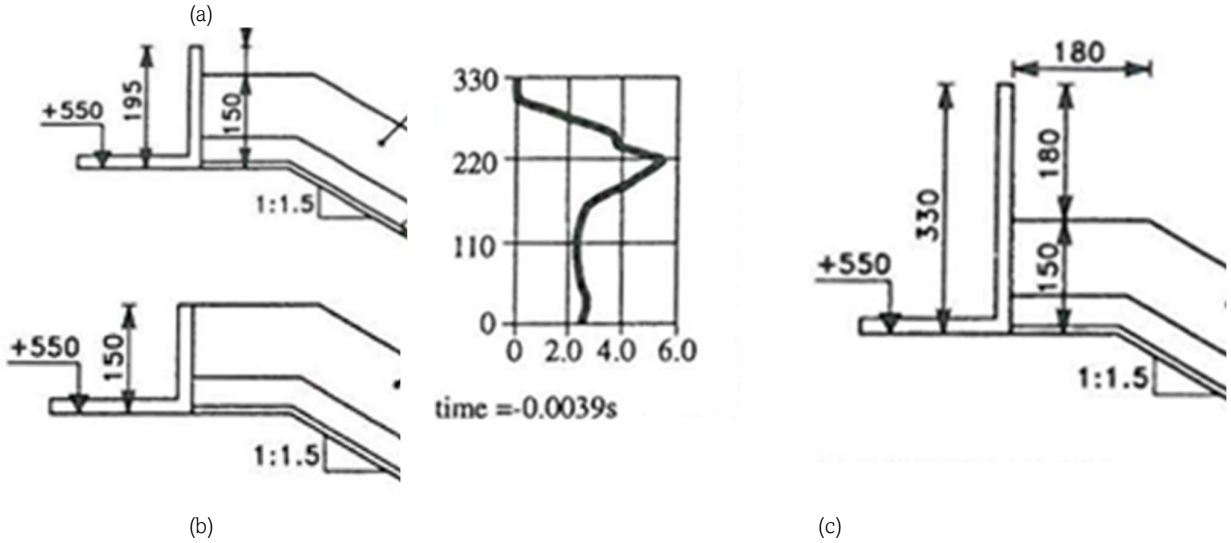

Figure 2.6 **Testing sections of breakwaters with crest walls in physical model tests. (a): Crest wall mostly sheltered by the armour layer. (b) Fully sheltered crest wall by the armour. (c) Partly exposed crest wall (with protruding element). Pedersen (1996).**

Van Gent and van der Werf (2019) performed tests to predict the wave loads on crest walls on top of breakwaters including the influence of oblique wave attack. In this study, an empirical formula is proposed that accounts for the so-called the virtual wave runup level. In this methodology, first the virtual runup is estimated, which is a function of the Irribaren number, wave height and a friction reduction factor for normally incident waves. Following, the total horizontal and vertical forces can be estimated by means of two formulae, which account for the height of the crest wall, the crest level of the armour layer and the virtual runup level to calculate the $F_{h2\%}$ and $F_{v2\%}$. In this formulation, the relative geometry of the crest wall and the armour crest is not accounted for, i.e., if a part of the crest wall is sheltered by the armour layer. In this type of empirical formulae, checking the range of validity is crucial before further application.

Jacobsen et al. (2018) introduced the issue of reproducibility of pressure peaks in physical model tests from point pressure records, Results from physical model tests showed that reproducing the same test three times yielded measurements of integrated forces over the crest wall that differ up to a factor of two in the raw signal (before any filter was applied). These forces are related to high frequency impacts and the fact that they are not reproducible, according to this study, indicates that there is a stochastic part in generating shock pressures. Lastly, regarding the limited time-efficiency of the numerical model Jacobsen mentioned that simulation of up 700 waves was in the order of days, and simulating only the higher waves for the estimation of forces could be a solution. However, a priori determination of which wave height is responsible of the 1% exceedance force is still uncertain.

Previous studies were carried out previously at the HE lab of TU Delft to study wave forces on emergent crest walls in similar experimental setup to the one of this study. Specifically, the setup of Veringa (2023) quantified the pressure distribution on emergent crown walls. The water level becomes relevant in this study, and in particular the distance between the still water level and the base level of the crest wall, the so-called foundation level, Fc. For Fc = 0 the free surface coincides with the base level of the crown wall. For Fc > 0 the crown wall is emerged. The findings of this study suggest that the triangular distribution of the uplift pressures described in the conventional design manuals for breakwater crown walls is accurate for the case of Fc=0 but overestimates the uplift force for emergent crest walls. Veringa (2023) also made observations with respect to the time lag that appears between the occurrence of maximum horizontal and maximum vertical uplift pressures. For the case when the base level of the crest wall is in contact with the still water level (foundation level Fc = 0) there is no time lag, so the recorded pressures peak simultaneously.

3. Methodology

3.1. Focused wave signal

The focused wave signal was defined according to the formulation of Tromans et al (1991), using a standard JONSWAP spectrum. The free surface elevation signal was then translated into the horizontal displacement of the wave board following the Biésel function for piston type wave makers (Hughes, 1993 after Biésel and Suquet, 1954).

In brief, the following steps were followed to generating the custom steering file for the focused wave:

1. Define the spatial coordinates in agreement with the physical flume of the experiment.

Prescribe the target JONSWAP spectrum (Equations 12 and 13), with peak enhancement factor, gamma = 3.3. Formulations and parameter values are obtained from Holthuijsen (2007). The frequency resolution was set as df = 0.001 Hz, with lower frequency cut-off, f_{low} = 0.1 Hz, and upper frequency cut-off, f_{upper}=1.5 Hz.

$$S(f) = \frac{\alpha g^2}{(2\pi)^4 f^5} \exp\left(-1.25\left(\frac{f_p}{f}\right)^4\right) \gamma^{\exp\beta}$$

Equation 12

$$\beta = \exp\left(-\frac{1}{2}\left(\frac{f - f_p}{\sigma f_p}\right)^2\right)$$

Equation 13

2. Apply Tromans et al. (1991) formulation for the timeseries of free surface elevation.

$$\eta = \sum_{n=1}^{\infty} a_n \cos(k_n x_n - \alpha \omega_n t)$$

Equation 14

Where, α: empirical celerity enhancement factor, a_n: wave amplitude per wave component.

The wave amplitude per frequency bin is calculated as follows:

$$a = a_{max}\left(Sdf\right) / m_0$$

Equation 15

The maximum wave amplitude in a series of N number of waves, a_{max}, is defined in Eq. 11.

3. In equation 14, prescribe the focal location, x_f, defined from the rest position of the wave board to the target focal point, where the wave signal is expected to develop the maximum wave height.
4. Apply Biésel function (Eq. 7) to transform the free surface elevation signal of the compact wave signal to the horizontal displacement of the wave machine (paddle stroke).
5. Apply taper to the stroke signal to smooth out any rapid transitions, accounting for three peak wave periods at the start and the end of the signal. This process of fading in and out the signal is done automatically by the wave-maker software for the tests of the irregular waves.
6. Export the paddle stroke signal in a readable format for the software used by the wave maker.

Regarding the operation of the wave paddle during the focused wave simulations, the active reflection compensation (ARC) system was switched-off during steering the signal and after the wave impacted the structure, the ARC was switched on again in between tests to achieve still water levels in the flume quicker, thus waiting times between tests could be reduced.

All tests made use of the six resistance wave gauges to record the incident wave height during the focused wave simulation. The target focused wave pre-focus and at focus are illustrated as timeseries (Fig. 3.1 b and c) and as spatial distribution (Fig. 3.1 a) along the flume figure 3.1. Specifically, figure 3.1. (a) shows two snapshots in the flume, one at 20 seconds prior to focusing (blue line) and one at the moment of focusing (red line). The red line with the wave at focus shows that the wave signal has reached the maximum wave height. The evolution of the wave shape a few seconds prior to focusing can be seen in figure 3.1 (c), when the wave shape is plotted spatially at times t = 5, 2 and 1 seconds prior to focusing. Note that for the focused wave, wave reflections from the structure are not relevant as the focused wave crest is essentially the first to reach the structure, and the main wave forcing – there is not second incoming wave field, as each steering file contains one wave signal. However, for simulation of the irregular waves the arrays of three wave gauges placed in the flume should be used to separate the incident to the reflected wave considering for example the introduced methodology by Zelt and Skjelbreia (1993), Andersen and Eldrup (2021), or de Ridder et al (2023). The focused wave realised in the flume can be seen in figure 3.2 (a) as it propagates through the wave gauges placed away from the structure. In figure 3.2 (b) a wave front propagating towards the armour slope during the irregular time series is shown in figure 3.2 (b).

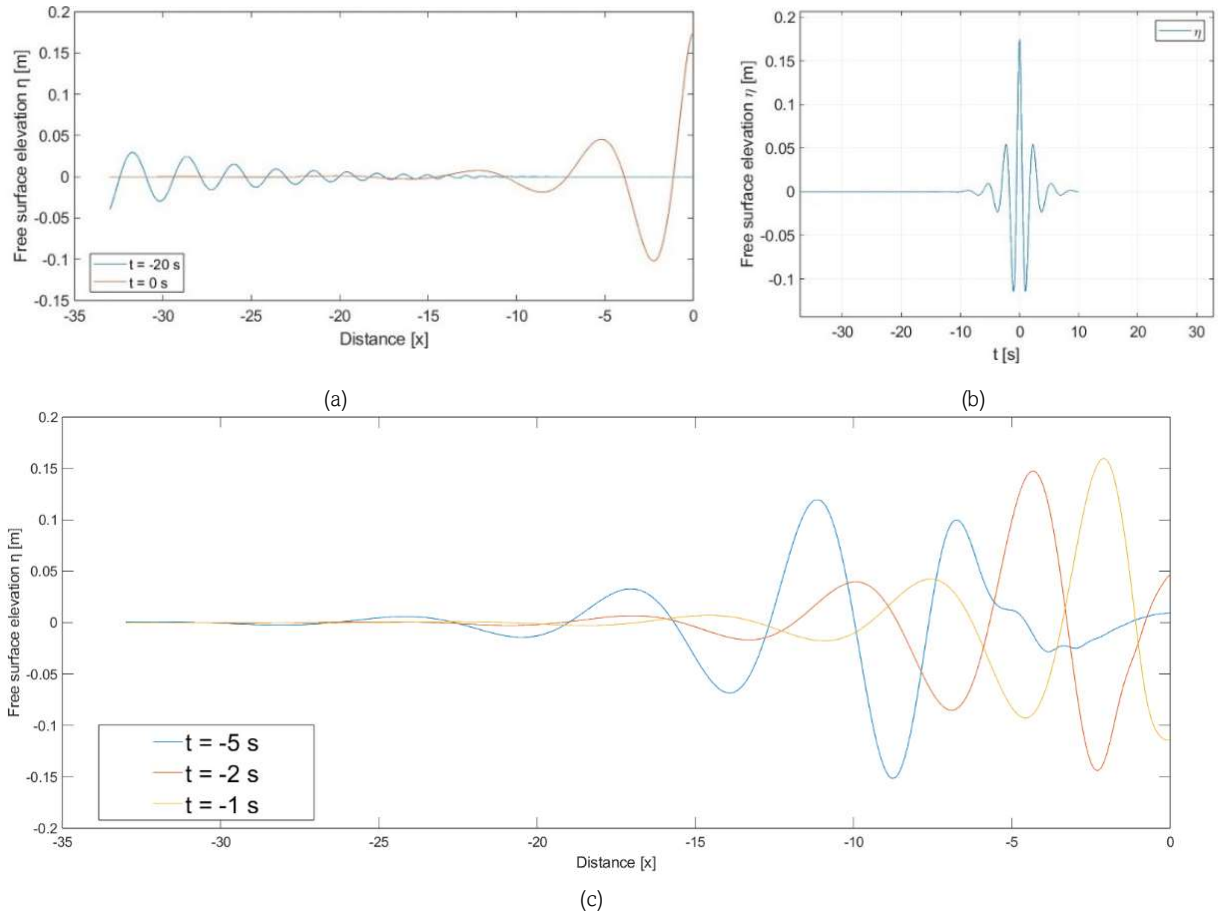

Figure 3.1 Focused wave as predicted by the linear wave theory. (a) Spatial evolution of focused wave, at t = 20 s prior to focus (blue line) and at focus, t=0 s (red line). (b): Free surface elevation timeseries at the focal point. (c): Spatial evolution of focused wave signals at t = 5 s prior to focusing (blue line), t = 2 s prior to focusing (orange line), and t=1 s prior to focusing (yellow line).

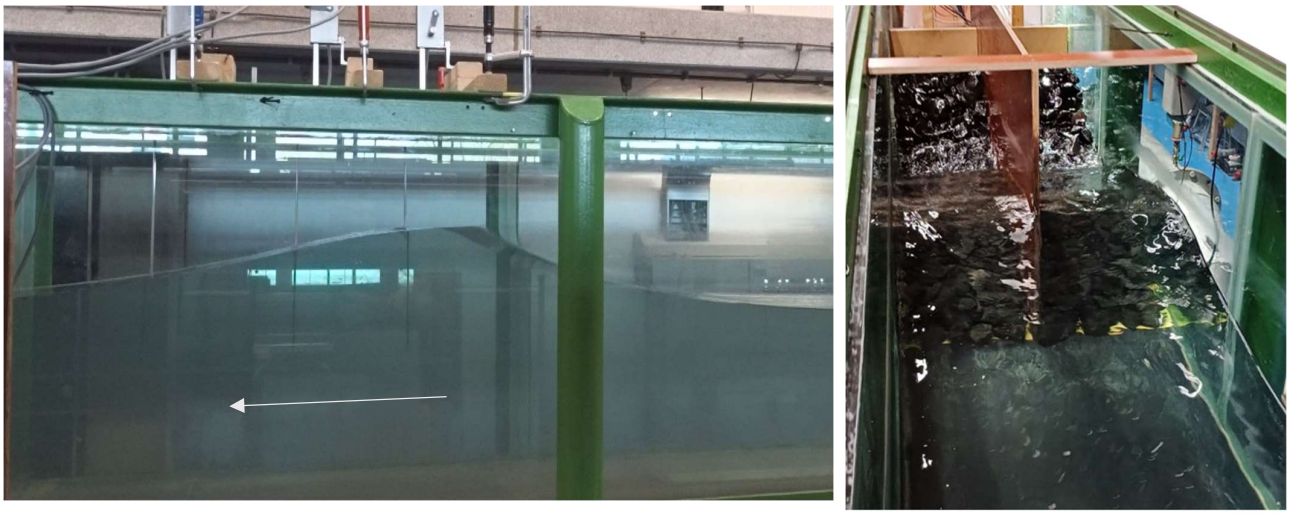

(a) (b)

Figure 3.2 Wave propagation in the flume. (a): Side view of the flume while focused wave propagates at the offshore measurement location. Arrow is pointing the propagation direction. (b): Front view of the testing section during irregular wave tests prior to a wave impacting the slope.

3.2. Experimental Setup and test programme

The experiments were performed in the wave flume of the HE Lab of TU Delft between 11-12th of April 2024. The flume consists of glass side walls supported by metal frames. The effective length of the flume used for this setup is about 35.0 m. The cross-sectional dimensions of the flume are 0.79 m width and 1.00 m height, with typical working depths: 0.5-0.7 m. The flume is equipped with a piston-type wave machine, including an ARC system. In this study, reflections from the structure are not relevant, since the time series last less than 2 minutes, and essentially 2-3 waves reach the structure. Nevertheless, measurements from all gauges are used to record the wave signal. The set up includes a separation wall, and slopes on both sides (Figure 3.2 b). This configuration is built so that two separate crest walls are tested. One side was instrumented with pressure sensors (Appendix A) and the other one with a proximity sensor which recorded the horizontal displacement at the leeside of the crest wall. Regarding the testing section (Figure 3.3 – 3.5), the armour slope is 1:2 with basalt covered in epoxy, dn50=0.053 m and grading d85/d15 = 1.38. The core of the breakwater consists of stones with dn50 = 0.9 cm and a grading d85/d15 = 2.03. At the armour crest the height of the armour is 0.12 m and 0.20 m wide. On the slope, the armour width is about 0.09 m. The model crest wall was 0.22 m high and 0.30 m wide.

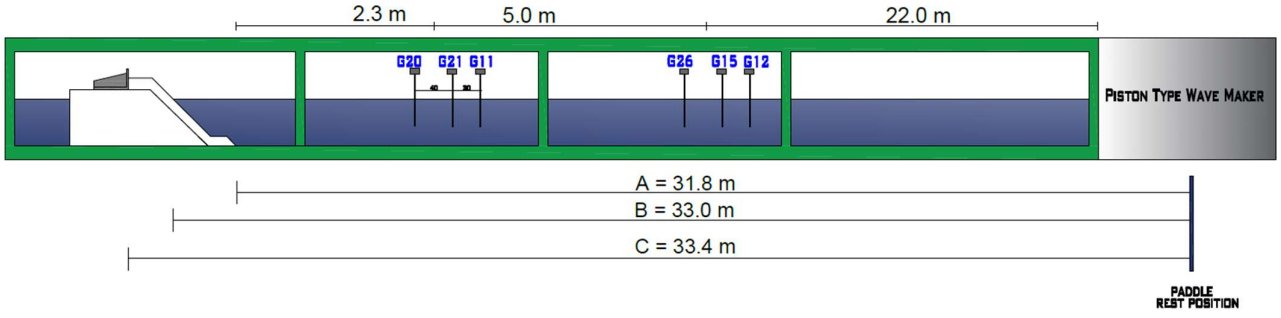

Figure 3.3 Physical flume and gauge deployment. Distances, a, b, and c, indicate focal lengths from the paddle mid points to the toe, intersection of waterline and armour, and crest wall. Distances between the gauges at the toe are 0.40 and 0.30 m.

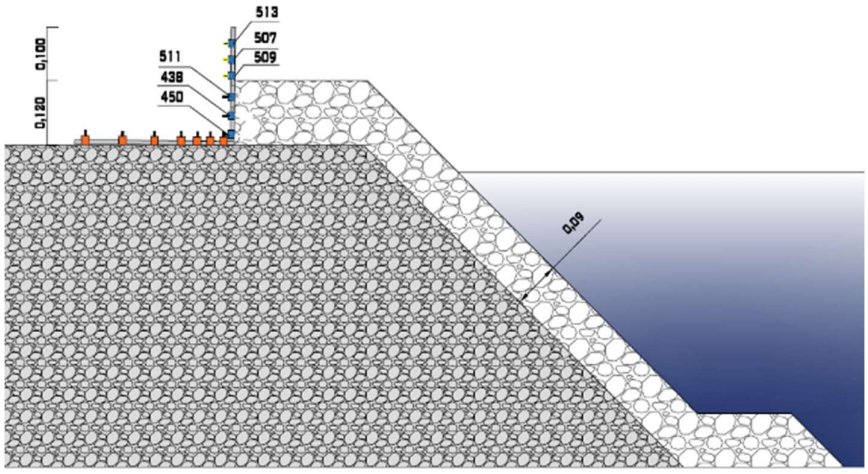

Figure 3.4 Testing section (a) Geometry and pressure sensors deployment.

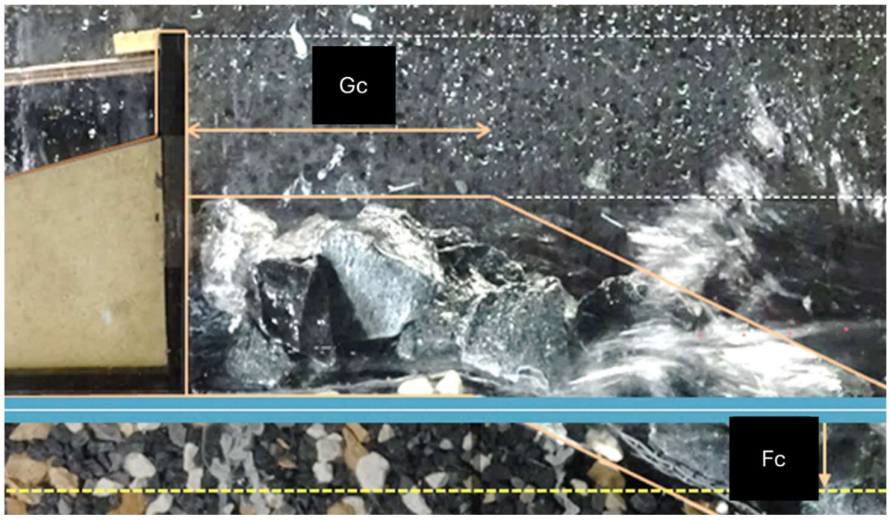

Figure 3.5 Experimental set up in the flume: Still water level corresponding to zero foundation level (blue line), the still water level corresponding to an emerged crest wall (yellow line), while Fc denotes the foundation level.

Table 1 Test programme overview.

Test Programme	Description	Number of tests
Test Series A & B	Calibrating the wave height of the signal in the laboratory flume.	10
Test Series C	Wave impact tests, focusing at the structure.	13
Test Series D	Wave impact tests, focusing at the structure, varying steepness, and water level.	6
Test Series E	Wave focusing at a measurement location offshore.	11

Table 2. Parameter Range in the test programme.

Parameter	Parameter range
Focal Distance from paddle rest position, x_f [m]	24.0 – 37.87 m
Incident wave heights recorded at the toe, H [m]	0.17 - 0.32 m
Peak wave period, Tp [s]	1.55 and 2.53 s
Celerity enhancement factor [-]	1.00 – 1.06

4. Results

4.1. Focused wave signals in the flume

This section presents results and observations from the recorded focused wave signals at the flume. Specifically, results are presented from the series of focused wave tests that aimed to reproduce a wave impact at the structure as illustrated in figure 4.1 and 4.2. Several objectives motivated the choices of the parameter space in this test series. The focal location x_f=32.9 m, roughly corresponded to the distance from the resting position of the paddle to the intersection of waterline and slope of the armour layer (fig. 3.3). Three tests prescribed the focusing to occur at the crest wall, i.e., x_f = 32.9 m, two tests prescribed a more seaward focal point, located about 2 m offshore from the toe of the structure, i.e., x_f = 30.5 m, so the measurement locations at the toe could better capture the focused wave shape. Eight tests used a focal point somewhat seaward of the water line, but still on the armour slope, i.e., x_f = 32.5 m, which was visually found to best reproduce a wave impact at the crest wall.

During the impact tests a downstream focal shift was observed in the wave records. Due to the limited wave gauges, and limited test programme, this focal shift was not systematically quantified. However, this observation was used when the focusing was aimed at the intersection of waterline and armour layer, by prescribing a focal distance upstream of this intersection, i.e., towards the toe of the structure, the shift accounted for 5% of the offshore wave length, a wave impact was visually observed and confirmed via the records of displacement of the crest wall and video. A further upstream shift of the focal distance by 15% of offshore wave length from the true position of intersection of waterline and armour did not yield a wave impact at the wall.

The physics of a focused wave impact at the testing section start with a deep trough approaching the structure, followed by small crest and finally the major focused wave that partly breaks on the armour slope and eventually strikes the protruding part of the crest wall generating the wave impact (Figure 4.1). The wave signals of the impact test series were targeted to correspond to $H_{0.1\%}$ and $H_{0.01\%}$ of a Rayleigh distributed irregular sea state.

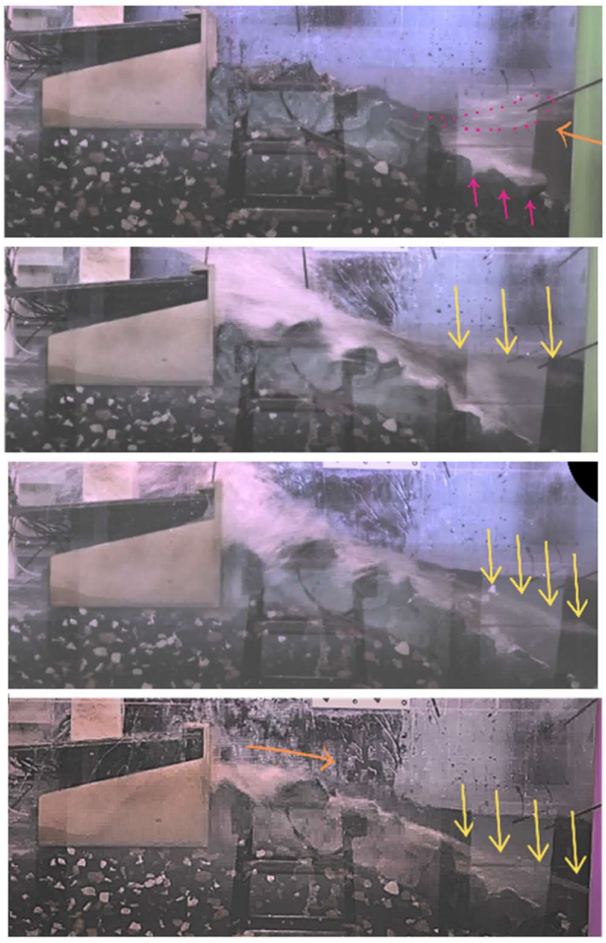

Figure 4.1 Sideview of the testing section.

Top to bottom:

i: Broken crest running up the armour layer, pink dots indicate air entrainment and pink arrow indicate air layer between the armour layer and the flow.

ii: Wave impact, yellow arrows indicate the water elevation.

iii: Same wave impact, yellow arrows indicate water level decrease at the armour.

iv: Run down phase at the armour crest (orange arrow) and armour slope (yellow arrows).

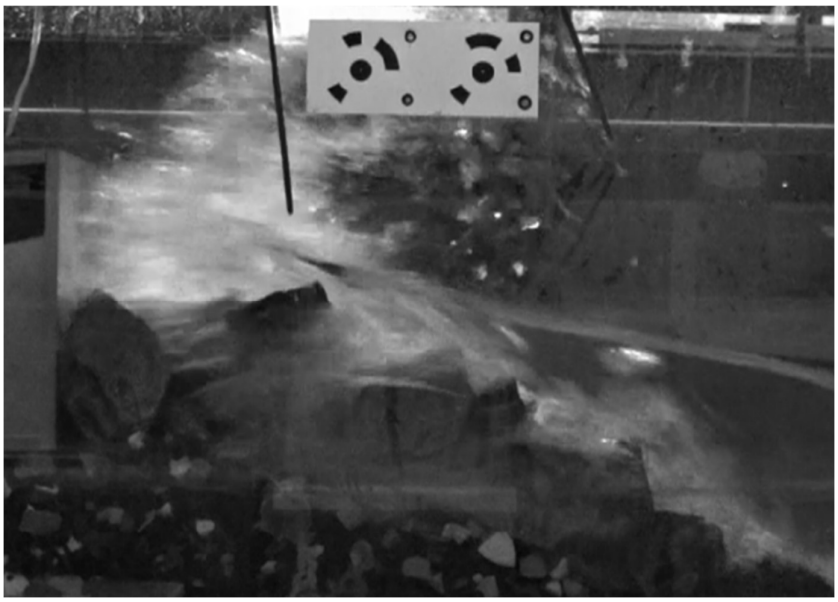

Figure 4.2 Close up wave impact at the crest wall during a focused wave test.

Table 2 Incident wave heights from focused wave impact tests, corresponding Rayleigh distributed random sea state, Hs = 0.15 m.

Test	Incident wave height at the toe, gauge G21
C001/1	Hi=0.28 m ≅ $H_{0.1\%}$
C002/1	Hi=0.31m ≅ $H_{0.01\%}$
C003/1	Hi=0.31 m ≅ $H_{0.01\%}$
C004/1	Hi=0.31 m ≅ $H_{0.01\%}$
C005/1	Hi=0.32 m ≅ $H_{0.01\%}$
C006/1	Hi=0.28 m ≅ $H_{0.1\%}$

The sensitivity of the wave signal towards the focal point and the celerity enhancement factor is illustrated in figure 4.3 (a) and (b), respectively. Timeseries are recorded at gauge 20, which is located 2.0 m from the toe of the structure. From figure 4.3 (a) it can be seen that the test aiming to focus at the intersection of water line and armour slope, i.e., x_f = 32.9 m the signal is less developed in terms of max wave height, compared to the one with shifted focal point offshore, i.e. 32.5 m from the paddle rest position (green timeseries in figure 4.3 (a). This focal point, xf = 32.5 corresponds to a location on the armour slope between the waterline level and the before the toe and was used for the majority of this test series. Sensitivity with respect to the celerity enhancement factor, alpha, indicates that an increase from 1.02 to 1.04 leads to a more asymmetric shape, but also a significantly higher crest elevation, i.e. H= 0.27 m to H= 0.31 m, as it can be seen in figure 4.3 (b). A similar observation can be made in figure 4.4, where an increase of alpha from a=1, to a=1.02 led to an increase in wave height and sharper crest, for focusing at x=32.5 m.

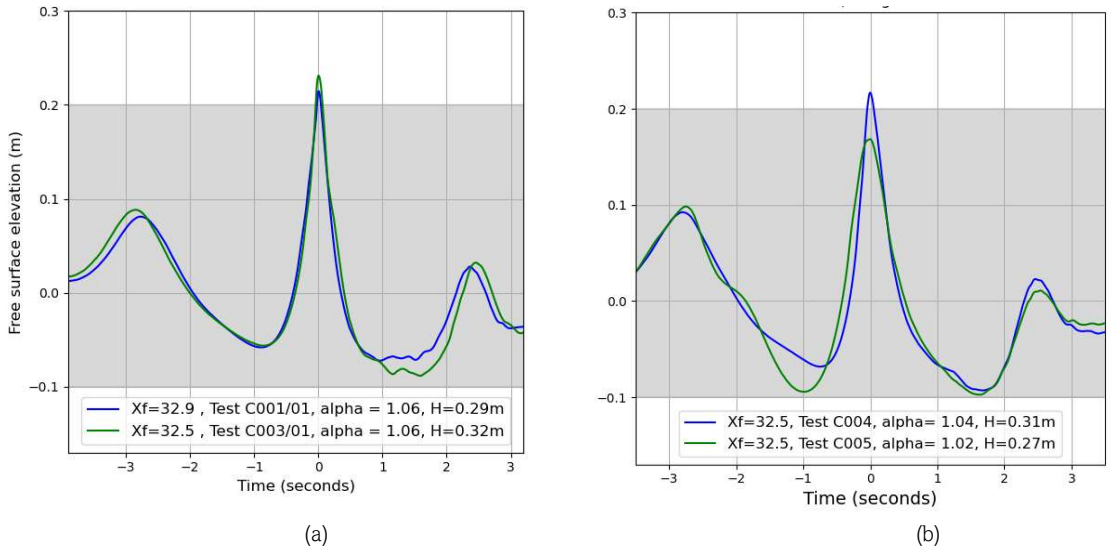

Figure 4.3 Free surface elevation timeseries, measured at the toe of the structure showing: (a) the effect of a shift in focal distance, xf in meters from the paddle rest position, and (b) influence of celerity enhancement factor, all recorded at gauge 20.

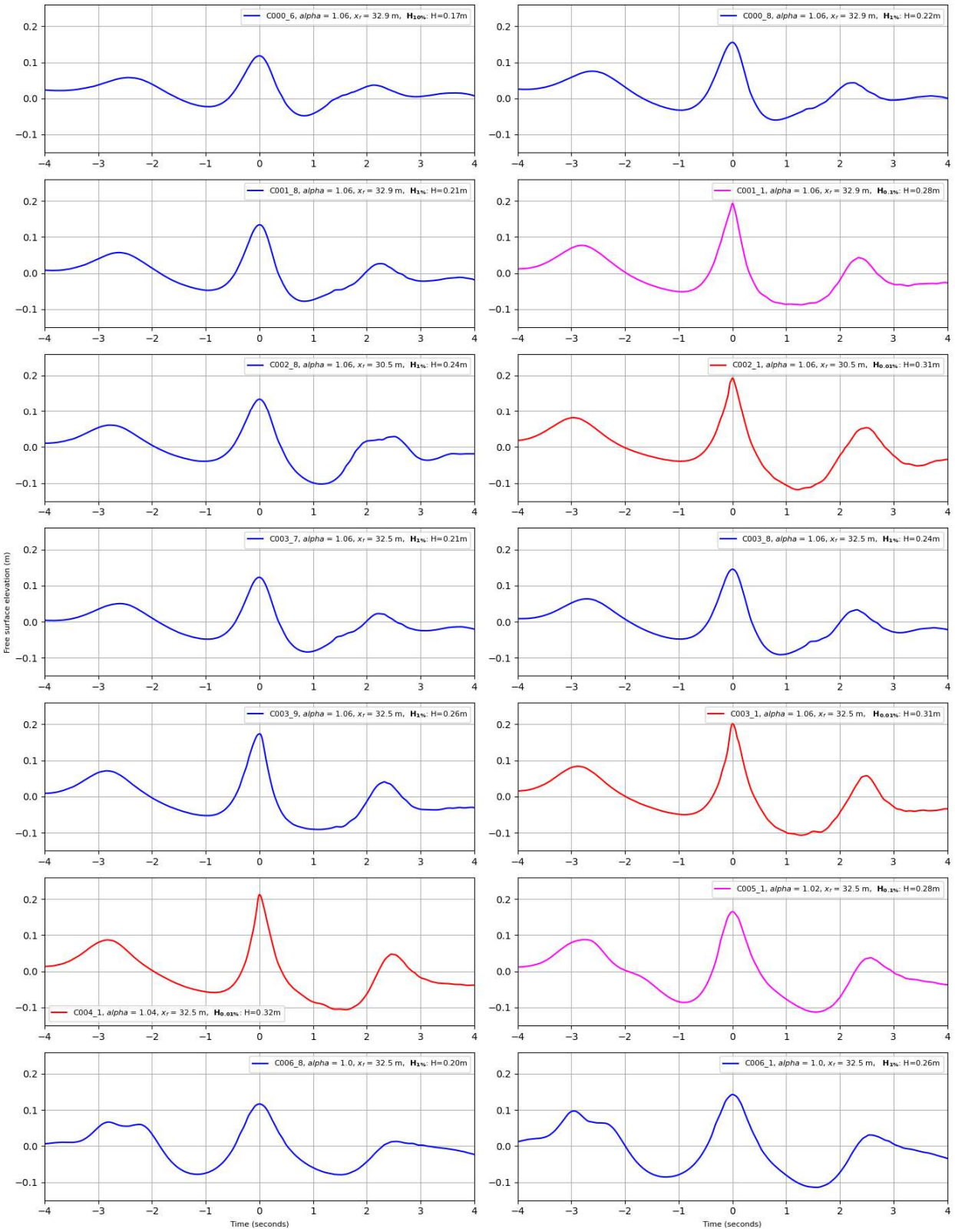

Figure 4.4 Measured focused wave signals at the toe of the structure, Gauge 'G21'. Correspondence to $H_{10\%}$ and $H_{1\%}$ (blue line), $H_{0.1\%}$ (magenta line) and $H_{0.01\%}$ (red line). Legend indicates focal distance, xf, per test measured from the paddle rest position, celerity enhancement factor, alpha, and the gauged maximum wave height during focused wave tests.

4.2. Hydraulic response under focused wave attack

4.2.1. Pressure signals

This section presents the pressure records and resulting integrated forces acting upon the front wall and horizontal face of the structure under focused wave attack, and following a comparison is conducted relative to the pressures recorded during the irregular wave timeseries. Six pressure gauges were placed on the front wall to capture the wave impact and seven pressure gauges were placed on the horizontal plate, where uplift pressures were recorded. The acquisition frequency of the pressure transducers is 100 Hz[1].

Pressure signals for the focused wave tests are illustrated in Figure 4.5, measured at the front wall of the model crest wall. Specifically, the focused wave heights recorded correspond to $H_{0.1\%}$ and $H_{0.01\%}$ of the Rayleigh distributed irregular sea state with Hs = 0.15 m, i.e., H = 0.28m and H = 0.32 m. Results indicate that the first sensor placed above the armour crest (sensor indicated in orange line and arrow in Figure 4.5) consistently recorded the highest peak pressures. That observation is reasonable as this sensor is more exposed to wave impacts as it is not sheltered by the armour layer. The pressure gauge placed immediately above measured significantly lower pressures (shown in blue line and arrow in Figure 4.5). According to the results, the pressure recorded at the first exposed to wave action sensor, was a factor two larger than the pressures measured in the two neighbouring sensors (i.e., pressure gauge 507 placed above and pressure gauge 511 placed below). This can be seen in Figure 4.5 (a) and (c). Another observation is that the same wave height at the toe of the structure can lead to significantly different impact pressures (see Figure 4.5 (a) and (d)).

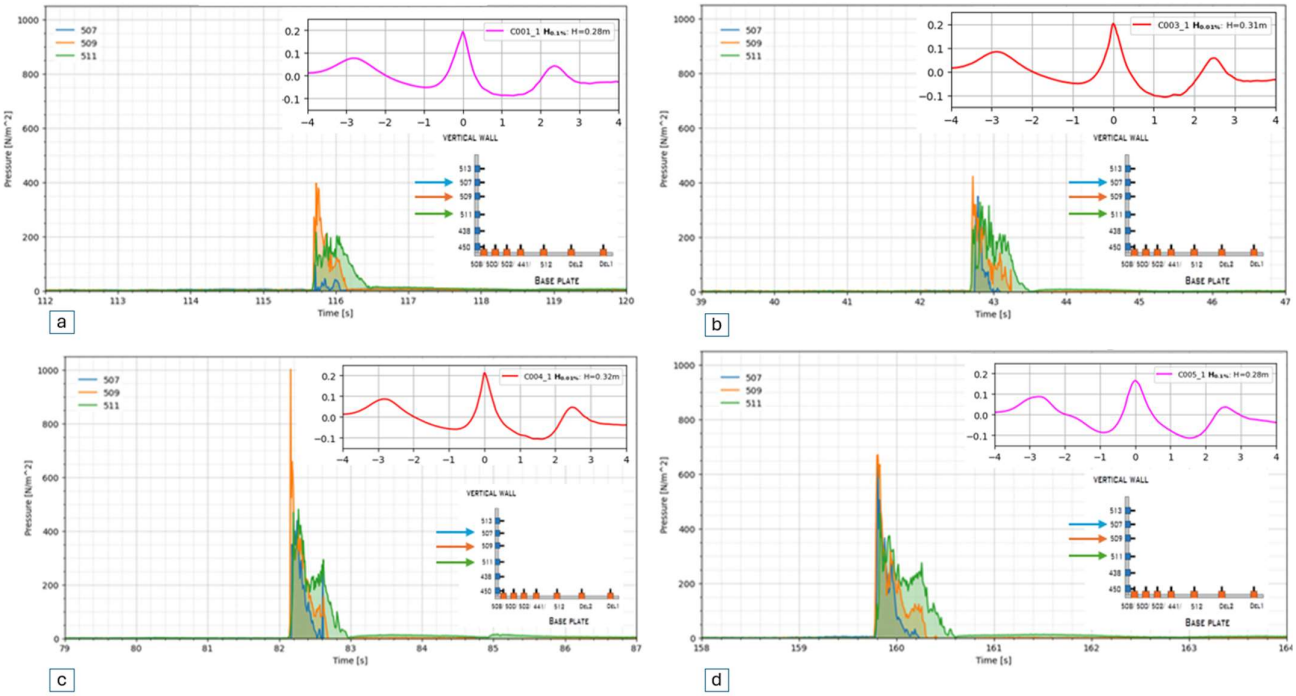

Figure 4.5 Pressures measured at the vertical wall under focused wave attack; pressure sensors, 507 (blue), 509 (orange), 511 (green), Test numbers, focal locations, xf, and celerity enhancement factors, a, as follows: a) Test C001, xf = 32.9 m, a = 1.06, Hi = 0.28 m, b) Test C003, xf = 32.5 m, a = 1.06, Hi = 0.31 m, c) Test C004 , xf = 32.5 m, a = 1.04, Hi = 0.32 m, and d) Test C005, xf = 32.5 m, a = 1.02, Hi = 0.28 m.

[1] For more information about the process of calibrating the pressure sensors the reader is directed to the work of Veringa (MSc Thesis, 2023). Type of transducer used is HKM-375(M).

Signals of uplift pressures during the same focused wave tests presented in Figure 4.5 as recorded on the front wall are now presented as recorded at the horizontal surface of the crest wall (Figure 4.6). A close observation of the dataset reveals that during both the primary and the secondary peaks of the pressure signals at all instances of Figure 4.6, the maximum uplift pressures are recorded at the most seaward sensor (blue line in the timeseries and blue arrow in the pressure gauge deployment). The pressure signals are not filtered for the present analysis, however analysis showed that a down sampling to 50 Hz influences the obtained peak pressure, especially in pressure records as Figure 4.6 (d). Focused wave heights with maximum height at the toe in the range of H = 0.28 - 0.32 m, corresponding to $H_{0.1\%}$ and $H_{0.01\%}$ led to peak (point) pressures at the most seaward pressure gauge within the range of 8 – 11 N/m^2 (Figure 4.6).

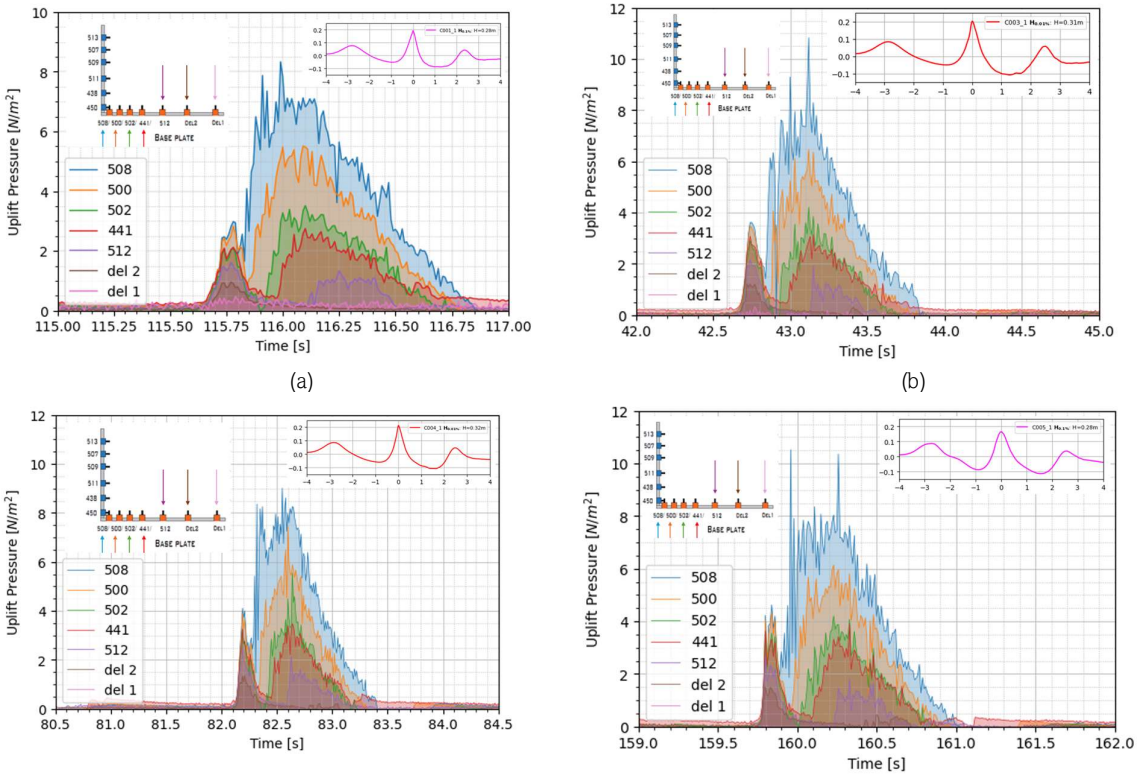

Figure 4.6 Pressure signals of uplift pressures on the base plate of the crest wall for focused wave signals, along with the corresponding recorded incident wave at the toe of the structure. (a) Test C001, Focal distance, xf = 32.9 m, Wave celerity factor, a = 1.06, Incident wave height, Hi = 0.28 m. (b) Test C003, Focal distance, xf = 32.5 m, Wave celerity factor, a = 1.06, Incident wave height, Hi = 0.31 m. (c) Test C004, Focal distance, xf = 32.5 m, Wave celerity factor, a = 1.04, Incident wave height, Hi = 0.32 m (b) Test C005, Focal distance, xf = 32.5 m, Wave celerity factor, a = 1.02, Incident wave height, Hi = 0.28 m.

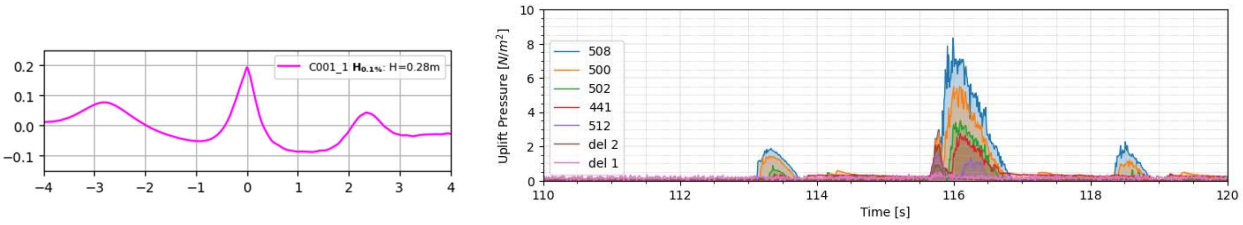

Figure 4.7 Focused wave signal (a) and resulting signal of uplift pressures during focused wave attack. Test C001/1.

A short series of tests were performed with increased wave steepness (Test Series D). Specifically the wave steepness in these tests was, $s_{o,p}$ = 4.0 % with the wave peak wave period T_p = 1.55 s. The increased wave steepness led to severe steepness induced breaking as can be seen in figure 4.8, creating the so-called whitecaps before the focused wave reached the structure. This steepness- induced breaking resulted in shorter wave heights at the toe compared to the target. This series of tests with increased wave steepness comprised three tests with a foundation level Fc = 0.03 m and three tests with an increased water level, i.e. foundation level of Fc = 0.01 m. For this series of six tests, the pressure signals recorded at the base of the model crest wall are compared for the two varying water levels under focused wave attack in figure 4.9. and resulting pressure distribution is presented in the next paragraph.

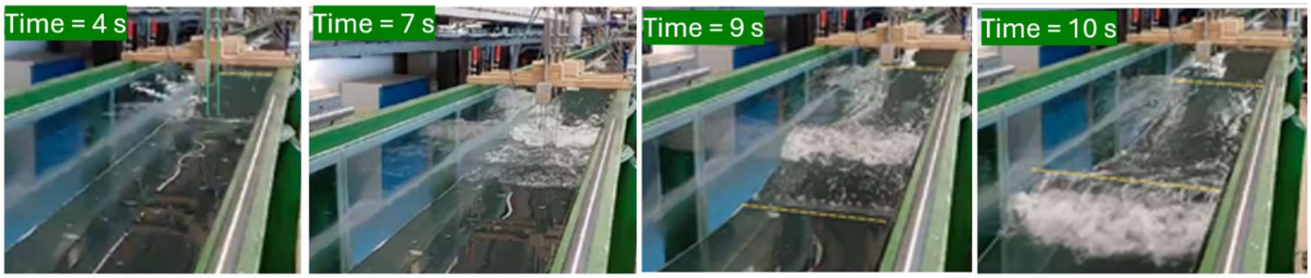

Figure 4.8 Steepness induced wave breaking. At t = 4 seconds the wave front still has the crest intact with a deep preceding trough, indicated in cyan vertical lines. At t = 7 s the crest starts to break and then propagates as a broken wave front.

Figure 4.9 presents the pressure records from the most seaward sensors located on the base of the model crest wall during focused wave attack – as the sensors placed on the leeside yielded records close to zero. A comparison between figures 4.9 a) and b) shows that the peak recorded (point) uplift pressure recorded at the most seaward sensor was about a factor 2 higher when the water level is increased by 0.02 m.

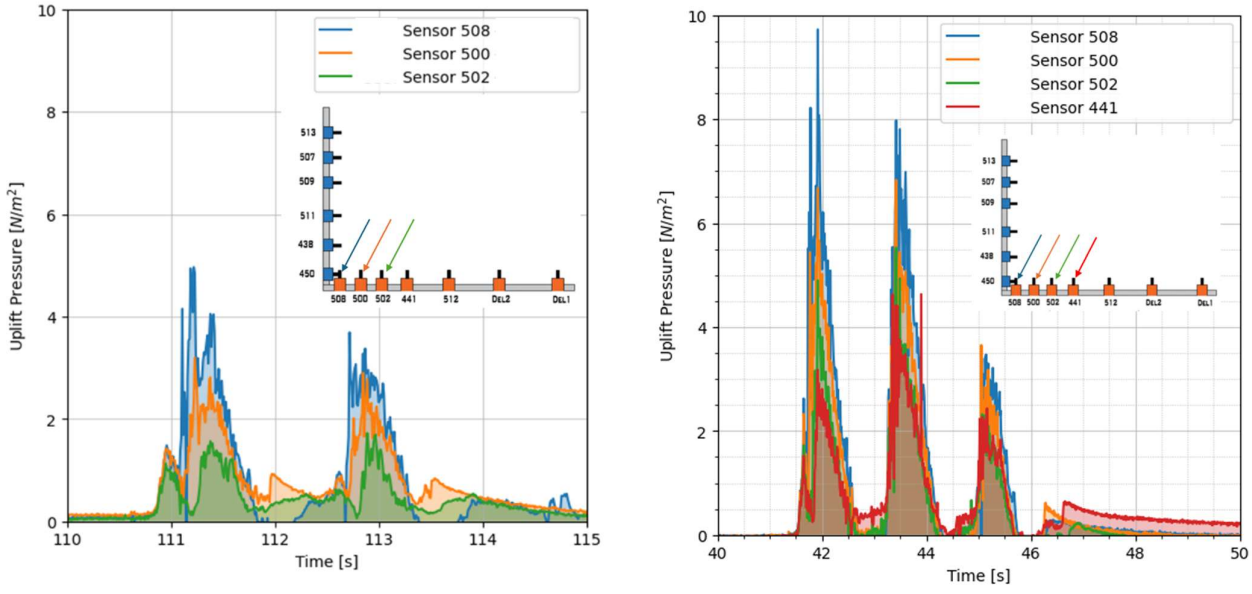

(a) (b)

Figure 4.9 Uplift pressure records from focused wave tests with same focal length in different water levels. (a): Foundation level, Fc = 0.03m, recorded incident wave height at the toe Hi = 0.25 m. (b): Foundation level, Fc = 0.01m, recorded incident wave height at the toe Hi = 0.23 m. Pressure records: from pressure gauge 508 (located seaward, blue line), pressure gauge 500 (orange line), pressure gauge 502 (green line) and pressure gauge 441 (red line, only in panel b).

4.2.2. Pressure distribution during focused wave attack

Here, pressure distributions are presented for two tests of focused wave tests with varying water depths to illustrate the influence of water level variation and in particular of the foundation level in the distribution of uplift pressure at the base of the crest wall (Figure 4.10). The aim of this comparison is to demostrate that even a short (focused) wave signal is also able to reproduce the change in the uplift pressure distribution at the base of the crest wall when the water level is increased (so the freeboard between the water level in the phreatic line and the base of the crest wall is reduced). Results showed, that for a foundation level of F_c = 0.03 cm the pressure distribution exhibits a sharp decrease in the first four sensors, i.e. 1/3 of the total length of the crest wall's base (from the seaward edge up to sensor 441) and at the remaining 2/3 of the base the distribution seems linear. Figure 4.10 (green line) shows that at about ¼ of the base plate's length, the pressure has reduced by half at the case of emergent crest wall. When the water level is increased by 0.02 m, so that the foundation level is Fc = 0.01 m, the pressure reduces to half at about 1/3 of the length of the base plate according to results (red line, Figure 4.8). Note that the forcing between these two focused wave tests differs not only in terms of the water level, but also in terms of steepness, with the test of higher steepness, Tp = 1.55 s being tested at the increased water level, while Tp = 2.53 s was tested in the lower water level. Focal distances, gain factor and celerity enhancement factors were the same for both tests. Recorded wave heights at the toe: $H_{i,\,C003/1}$ = 0.31 m, $H_{i,\,DCWL/01}$ = 0.23 m.

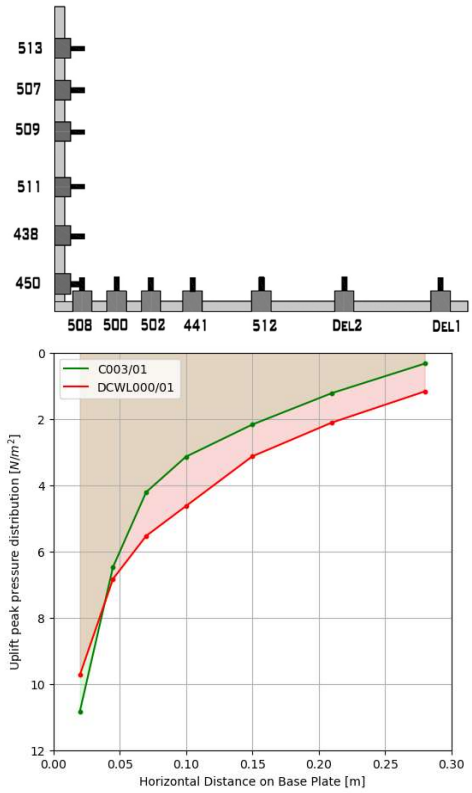

Figure 4.10 Pressure distributions at the base plate for two testing conditions with varying water levels, Fc = 0.03 m (Green line) with steepness, so,p =1.5 % and Fc = 0.01m (red line) with steepness so,p = 4.0 %.

4.2.3. Pressure rise times

The physics behind the decrease of rising times for higher pressures is explained in Cuomo et al. (2010) where rise times are plotted with respect to the peak force. Cuomo mentions that wave impulse should be seen as a finite quantity, therefore a more intense impact would occur in shorter rise times. Wave impulse is defined as the surface area below the pressure timeseries, during a pressure peak, which can be simplified as a tringle with the base being the rising time and the peak pressure being the height. Then the pressure impulse can be simply defined as the area prescribed by this triangle. This methodology was introduced by Mc Connell and Kortenhaus (1997). More recently, Chen et al. (2019) proposed a methodology to predict reaction forces on vertical walls with overhangs by using the impulse as the primary load variable, essentially by separating the quasi steady and impulsive components of the impact.

For the total of impact tests due to focused waves, the pressure rising times were determined, at the sensor which consistently recorded the maximum pressures at the vertical face of the crest wall, i.e., the first non-sheltered by the armour layer sensor in the vertical, and were then plotted against the corresponding maximum recorded pressures. It can be seen that higher pressures, consistently develop in shorter rising times.

Specifically, it can be seen that for all pressures above 500 N/m2, the rising times are always shorter than 0.05 s (Figure 4.11). At the same time, there was no impact recorded with rising time longer than 0.1 s. It should be mentioned that the shorter rising time coincides with the sampling frequency of the pressure gauge, at 0.01 s.

The rising times were calculated from zero pressure until the maximum is reached as can be seen in the examples shown in Figure 4.12. In case of double peaked pressure records (Figure 4.12, c), again the maximum peak is considered. This range of pressure rise times seems to be in agreement with the findings of Pedersen (1996) for partly exposed crest walls.

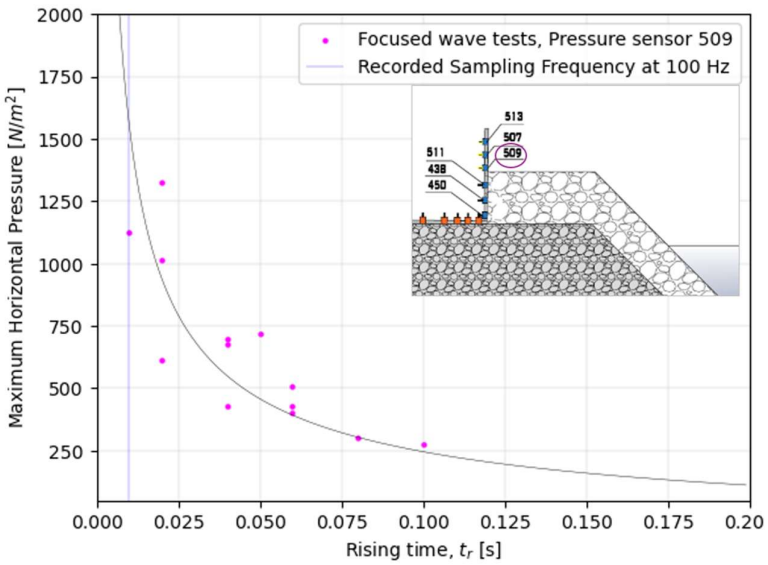

Figure 4.11 Rising times of the peak recorded horizontal pressures at pressure sensor 509 located at the front wall.

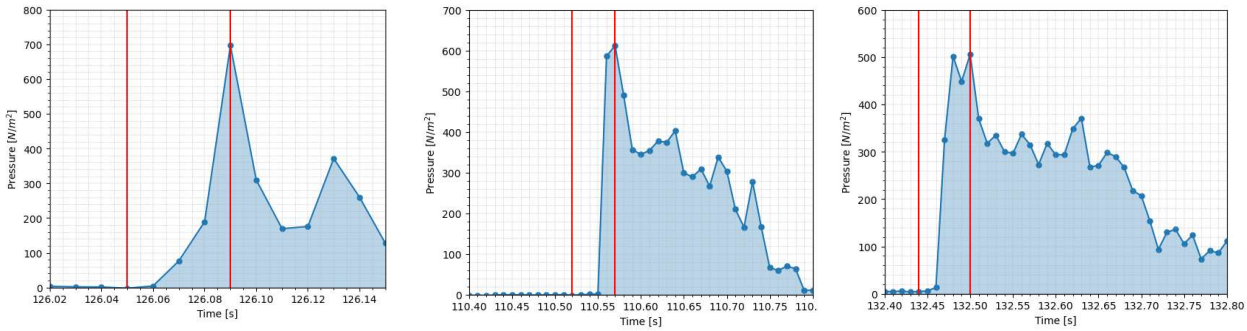

a b c

Figure 4.12 Examples of pressure records during focused wave tests and indication of rising times (red lines). Pressure rise times, t_r, and peak pressures, P_{max}: (a) t_r= 0.04 s, P_{max} = 696 Pa, (b) t_r= 0.05 s, P_{max} = 612 Pa, (c) t_r= 0.06 s, P_{max}= 506 Pa.

4.2.4. Sliding Failure

This section refers to the assessment of sliding failure during focused wave attack. Again, the physical process is the same, the focused wave starts to break on the armour slope and a wave jet impacts the crest wall, leading in some cases to a sliding failure. Displacement measurements were performed simultaneously to the pressure measurements as two identical crest walls were placed in the flume. The model crest wall at which the displacement was measured was free to slide (Fig. 4.13), but a critical weight was placed inside. The critical weight associated to a foundation level, Fc = 0.03 m calculated for the irregular wave tests was implemented here. For a wave period of Tp=1.55 s, wave steepness, $s_{o,p}$= 4.0 %, w_{crit} = 6.6 kg (including the weight of the wall), while for the longer waves of Tp = 2.53 s, $s_{o,p}$= 1.5 %, w_{crit} =20.2 kg. The sliding failure criterion in this case was defined based on a threshold of a displacement equal to 0.2 mm.

Figure 4.13 Model crest wall. Left panel indicates the metal plate where the proximity switch aimed to measure the displacement. Right panel indicates the displacement direction. Note this core material does not represent the one tested in these experiments.

The wave impacts that resulted in sliding failure were recorded during focused wave tests with wave heights at the toe equal to $H_{0.1\%}$ and $H_{0.01\%}$ of the Rayleigh distributed sea state for the tests with lower steepness, with focal distance x_f = 32.5 m measured from the rest position of the wave board. Results indicate that an increase in the celerity enhancement factor celerity enhancement factor alpha, from 1.02 to 1.04 led to a more severe displacement, indicating that the wave was better focused at the time of the impact. This is also shown in chapter 4.1., Figure 4.4, where the wave signal corresponding alpha value, a= 1.04, recorded a higher focused wave height at the toe of the structure, compared to other testing conditions with the same prescribed focal distance. Displacements recorded during steeper waves are shown in Figure 4.14 (b). This group of runs includes testing in two different foundation levels, varied by 0.02 m. For the tests where the water level was increased, the critical weight placed inside the crest was kept the same. The recorded incident wave heights at the toe of the structure for the tests with the largest foundation level (Fc = 0.03, Test group D), varied from H = 0.21 m - 0.25 m. A sliding failure was recorded only in the test with the higher wave height, H = 0.25 m. (Figure 4.14 (b), Test D000/1). The three tests performed at an increased water level show a larger displacement, which indicates that a higher water level results in more severe failure in terms of horizontal displacement, as seen in Figure 4.14 (b).

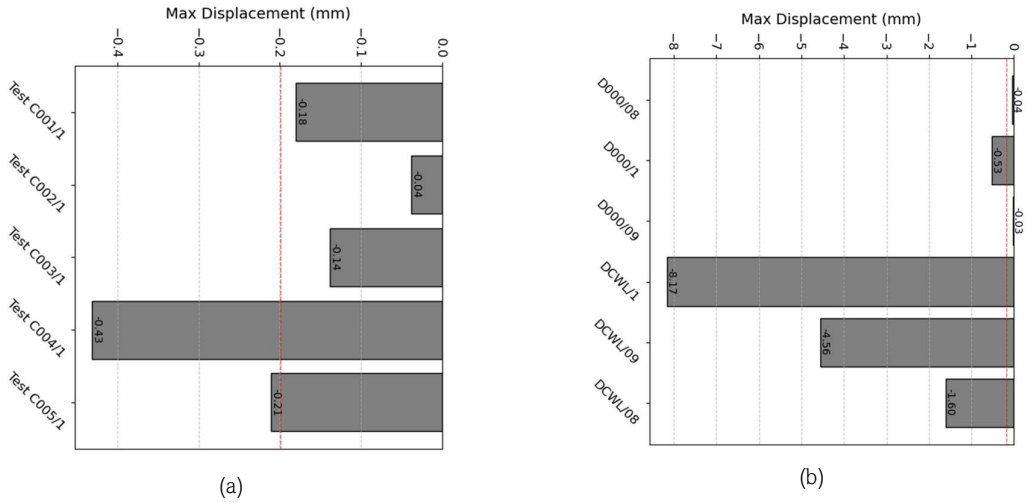

Figure 4.14. Horizontal Displacement of crest wall under focused wave attack. Red line indicates the sliding failure threshold, Δx=0.02 mm. (a) Maximum displacement per test. Incident wave heights for tests recording failure: C004: Hi = 0.32 m, C005: Hi = 0.28 m. Target wave period T_p=2.531s and F_c =0.03 m. (b) Target wave period T_p=1.55s.

4.3. Comparison of hydraulic response during focused and irregular waves

4.3.1. Pressure signals

Pressure signals obtained from the pressure gauges located on the crest walls were recorded during the simulation of a thousand waves. Two extreme events were selected, measured at the first exposed to wave action pressure gauge located in the front wall, i.e., $P_{H,\,irregular} = P_{0.2\%} = 658$ Pa which occurred at t = 675 s and $P_{H,\,irregular} = P_{0.5\%} = 509$ Pa, which occurred at t = 1775 s. The recorded wave height at the toe of the structure for both events prior to the wave impact was H = 0.28 m, accounting for the total signal.

Following, these two extreme pressures are compared to the peak pressures recorded during the focused wave attack. $P_{0.2\%}$ was best reproduced by a focused wave with maximum incident wave height at the toe, Hi = 0.26 m, resulting in point pressure recorded at the front wall, $P_{H,\,focused} = 678$ Pa. $P_{0.5\%}$ was found to be best reproduced by a focused wave with incident wave height at the toe, Hi=0.28m, and $P_{H,\,focused} = 506$ Pa. In this instance, the gauged wave height of the irregular waves (total signal) coincided with the incident wave of the focused wave, i.e. H = 0.28 m. The prescribed location for the focused waves was between the intersection of the waterline with the armour and the toe of the structure, specifically 0.5 m upstream the intersection of waterline to the structure. Expressed as a distance from the paddle rest position, which reads $x_f = 32.5$ m. Figure 4.15 illustrates the pressure signals recorded at the front wall overlapped for the focused and irregular wave test, for extreme event 1 in panel (a) and for extreme event 2 in panel (b).

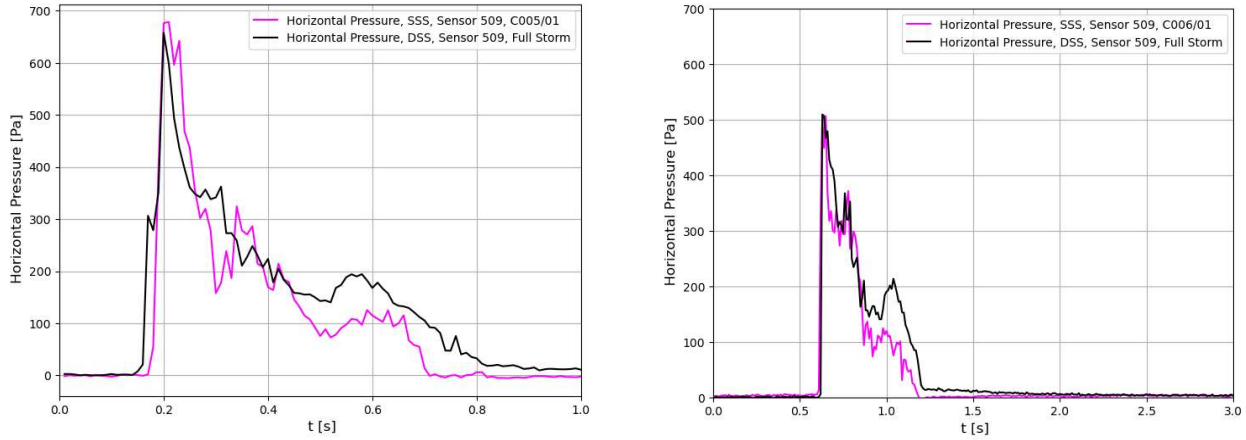

(a) (b)

Figure 4.15 Comparison of horizontal pressure signals between the Design Sea State (DSS: black line) and the focused wave signal (Substitute Sea State, SSS: magenta line) for (a) Focused wave-induced pressure and $P_{0.2\%}$ of the irregular wave-train, and (b) Focused wave-induced pressure and $P_{0.5\%}$ of the irregular wave-train.

Following, a comparison of the recorded uplift pressures is presented, as recorded from the most seaward pressure gauge. The extreme wave impacts considered before, leading to point pressure at the front wall corresponfig to $P_{0.2\%}$ and $P_{0.5\%}$ are analysed here with respect to the uplift pressures. Figure 4.16 illlustrates the pressure signals for both focused waves and irregular wave trains, indicating, that focused waves underestimate the peak uplift pressure on average by 20%. Both signals (irregular and focused) demonstrate a smaller peak before the occurrence of the major peak of uplift pressure. This smaller 'hump' in the pressure record is found to coincide with the occurrence of peak pressure recorded on the vertical face, by checking the associated time stamps of the record. This confirms the time lag that characterises the occurrence of peak uplift pressures in this type of structure. For both impacts, during the focused wave impact led to longer rise times and the peak pressures were lower. Additionally, there are a couple sharp pressure peaks that could be non physical, i.e. related to the content of air in the impact Figure 4.16, d. Also these peaks would have been filtered out if such post processing routine was implemented to adjust the data to a lower sampling frequency. This observation is also relevant for the results of the irregular sea state.

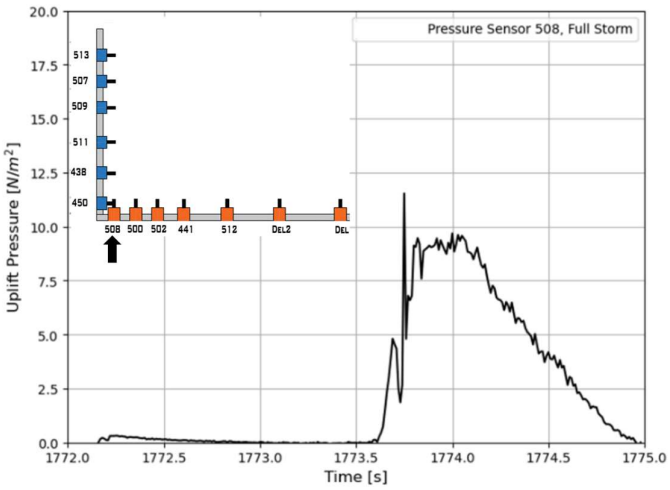

(a) Uplift pressure signal for random sea state, extreme event 1.

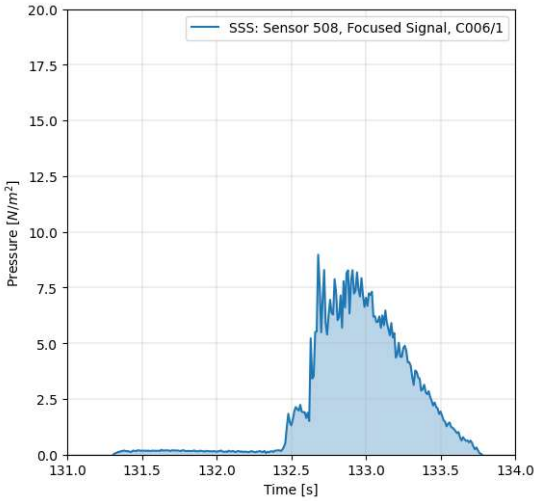

(b) Uplift pressure for focused wave signal, test C006/1.

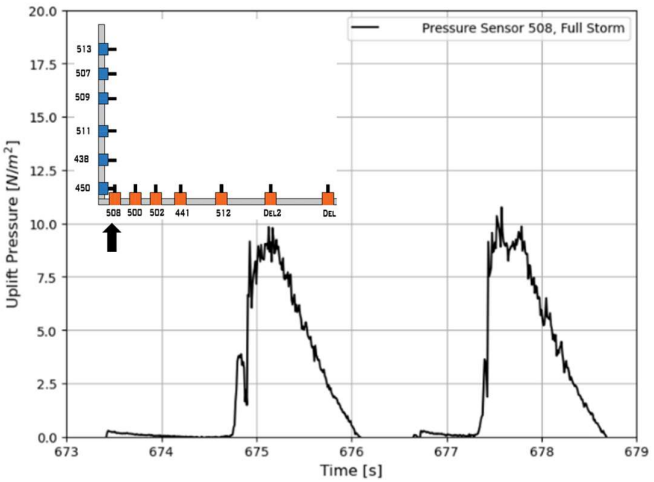

(c) Uplift pressure signal for random sea state, extreme event 2.

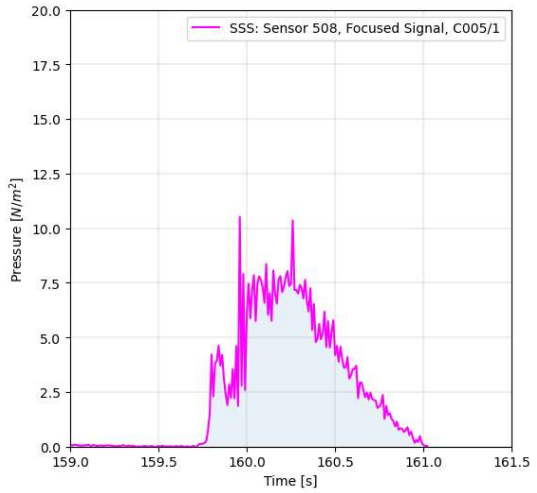

(d) Uplift pressure signal for focused wave signal, test C005/1.

Figure 4.16 Uplift pressure signals for extreme wave impacts for the irregular wave simulation $P_{0.2\%}$ (a) and $P_{0.5\%}$ (c) and uplift pressure signals during the focused wave attack in (b) and (d).

Table 3 Overview of wave parameters, focal characteristics, and water levels for tests with steepness $s_{o,p}$ = 4 %.

#	Test ID	Incident wave heights at gauge G15	Focal distance from paddle rest position.	Foundation level, Fc
1-3	D000, D001, D002	0.24 - 0.25 m	32.50 m	+ 0.03 m
4-6	DCWL_1, DCWL_2, DCWL_3	0.23 - 0.25 m	32.50 m	+ 0.01 m

4.3.2. Pressure distributions

In this section the analysis of pressure distributions is presented. Pressure distributions originating from focused wave simulations and simulations of irregular waves are illustrated. These distributions are derived from the point pressure gauges located at the front wall and the base plate of the crest wall (fig. 4.17 c).

The pressure distributions at the front wall are shown in figure 4.17 at the time instances when the extreme pressure corresponding to the second and the fifth extreme impacts are recorded in the irregular wave simulation comprising a thousand waves, $P_{0.2\%}$, and $P_{0.5\%}$. These are point pressure records, measured at the first sensor placed on the protruding part of the crest wall as shown in figure 4.11 and 4.17 (c) – namely the sensor 509. Comparison based on these two instances indicates that the pressures are well reproduced in the sensors placed in the sheltered part of the crest wall's front face, up to the critical sensor, where the maximum pressures are consistently recorded (fig. 4.17 a, b). Regarding the pressure distribution on the horizontal plate (Figures 4.17 d, e) it is observed that the focused wave impact underestimated the uplift pressures. This could be possibly attributed to the deep trough preceding the focused wave impacts prior to the main wave attack, which does not occur in the preceding waves during the irregular sea state.

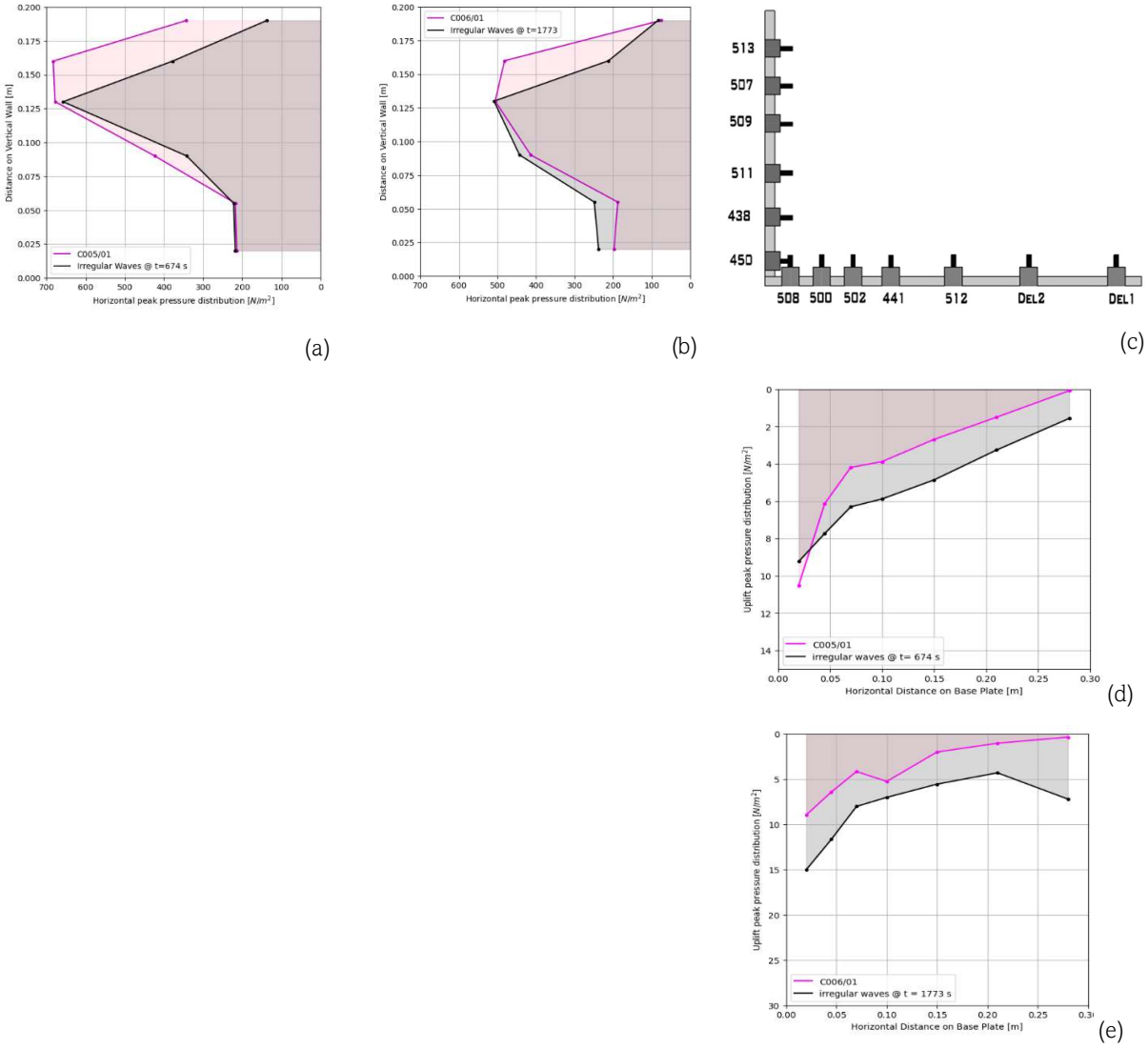

Figure 4.17 Pressure distributions at the time instance when peak impact pressures occured $P_{0.2\%}$ (t = 675 s) and $P_{0.5\%}$ (t = 1773 s) at the front wall (a) and (b) and base plate (d) and (e) during the irregular wave train (black) and focused wave (magenta).

4.3.3. Impact Forces

The comparison between the resulting forces on the crest wall during a wave impact induced by a compact, focused wave signal and an irregular wave train continues in this section with respect to the total integrated force acting upon the front face of the wall – the horizontal force, and the vertical force acting on the base plate. The impacts during the irregular wave simulation presented here correspond to the recorded peak pressures $P_{0.2\%}$ and $P_{0.5\%}$ from the sensor that consistently recorded maximum pressures, i.e., the first sensor exposed to wave action, located at the protruding part of the front wall, above the armour layer (figure 4.11). Pressure records are presented for all 6 sensors placed on the front wall and integrated forces are calculated based on simple Riemann summation, with extrapolation towards the edges of the wall.

For the extreme impact corresponding to pressure $P_{0.2\%}$ during the irregular wave test, the integrated force on the front wall is reproduced, with a margin of about 15% with the focused wave underpredicting the total force (Figure 4.18). Here, the recorded focused wave height at the toe was somewhat smaller compared to the wave height recorded prior to the impact during the irregular wave simulation. Specifically the maximum wave height at the toe during focused wave test: H = 0.26 m, and for the irregular wave train of a thousand waves, the total wave signal gauged at the toe reads a wave height H = 0.28 m prior to the wave impact that resulted in the second most severe impact in terms of pressure record, measured at the first exposed sensor of the crest wall. The comparison of integrated force with exceedance value $P_{0.5\%}$, where the wave height of the focused wave at the toe correspond to irregular wave trains (total signal), the response due to focused wave forcing in terms of total horizontal force is over estimated (Figure 4.19). This can be expected due to the second order effects as stated in the introduction, originating from the first order steering (absence of second order corrections).

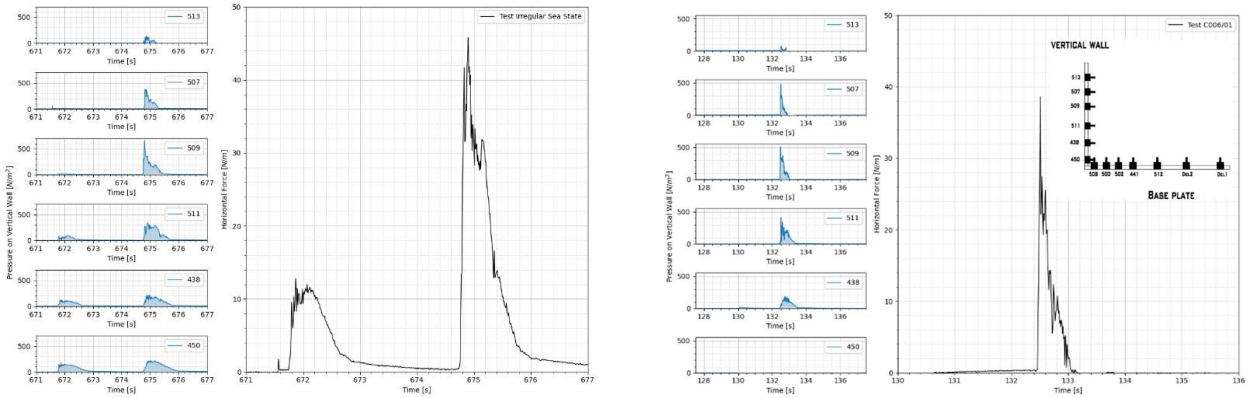

Figure 4.18 Impact pressures (blue) and integrated force (black) on the front wall, (a): irregular sea state, and (b): focused wave. Peak pressure recorded at the first exposed sensor, placed above the armour layer, corresponds to $P_{0.2\%}$ of the irregular signal.

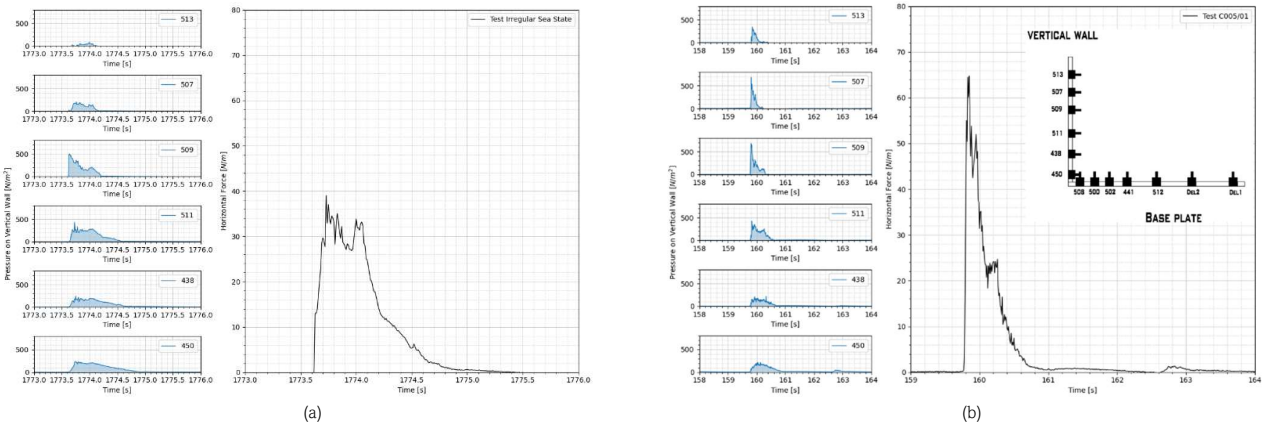

Figure 4.19 Impact pressures (blue) and integrated force (black) on the front wall, (a): irregular sea state, and (b): focused wave. Peak pressure recorded at the first exposed sensor, placed above the armour layer, corresponds to $P_{0.5\%}$ of the irregular signal.

5. Conclusions and Recommendations

5.1. Conclusions: Focused wave impacts & Comparison to irregular wave impacts

This project aimed to investigate whether compact, focused wave signals are able to reproduce extreme hydraulic responses in crest walls in comparison to loading by a series of a thousand irregular waves. The focused waves were steered and calibrated so that their maximum wave height corresponds to extreme exceedance percentages of a Rayleigh distributed irregular sea state, that is, the maximum wave in a thousand waves, and the maximum wave in 10.000 waves. Several focal distances were tested with the main goal to create a wave impact at the crest wall that is following assessed in terms of pressures and sliding failure. At the test series in which wave impacts are implemented, the recorded wave signals in the flume indicate a downstream focal shift, which was dealt with by prescribing a focal distance upstream the target of about 5 % of the offshore wave length.

The concluding remarks regarding the physics of wave impacts at crest walls when the impacts are generated by steering compact, focused wave signals can be summarised as follows:

- **Pressure distributions:** Peak pressures during the focused wave tests were consistently found to be greater at the pressure sensor located above the sheltered area of the crest wall (Figure 4.5). Peak uplift pressures were found to be greater at the most seaward edge of the base plate of the crest wall (Figure 4.6).
- **Uplift Pressures:** The distance between the phreatic line the core of the breakwater and the base plate of the crest wall was found to have a significant influence on the uplift pressure distribution during the focused wave tests (Figure 4.8). Specifically, the emergent crest wall with a foundation level of Fc = 0.03 m displayed a rapid reduction of the pressure profile towards the leeside of the base plate during wave impacts, while water level increase of 0.02m yielded a more linear uplift pressure distribution in the base plate of the crest wall.
- **Sliding Failure:** Horizontal displacements above the threshold indicating sliding failure were recorded for focused wave tests with wave heights corresponding to $H_{0.1\%}$ and $H_{0.01\%}$, of the irregular sea state, for both steepnesses tested (Figure 4.14), for the foundation level of Fc = 0.03 m, where the same critical weight was placed inside the crest wall as placed during the irregular sea state adjusted accordingly for the two steepnesses tested.
- **Water level change:** An increase of water level of 0.02 m for waves of the same steepness led to severe sliding failure (Figure 4.14, b) and an increase in uplift pressures by a factor 2 (Figure 4.9).
- **Types of impacts:** A compact wave signal, focused in the vicinity of the structure with a prescribed wave shape following the formulation of Tromans et al. (1991) was able to reproduce impact pressures of various types (Figure 4.12), for instance, single peak (impulsive) or double peak with an oscillating / quasistatic post-shock section and (non-impulsive) pulsating load, depending on the amount of air entrainment, the focus point relative to the structure, and how early the wave breaks on the slope.
- **Rising times:** There is a negative correlation between the pressure rising times and the magnitude of the recorded pressures measured at the front wall of the crest wall based on the data points acquired during the test series when waves were focused on the armour slope (Figure 4.11).
- **Time lag:** A time lag is consistently recorded between the peaks of the impact and uplift pressures (Figures 4.5 and 4.6).

All in all, results of this study showed that compact, focused wave signals propagating in flat bed and generated in deep water regime can be used in combination with test series of irregular wave tests in physical model tests to reproduce the physics of wave impacts and extreme hydraulic responses in crest walls, in terms of impact pressures and sliding failure. Specifically:

- **Peak Pressures**: The peak impact pressures recorded during the irregular sea state of a thousand waves, namely $P_{0.2\%}$ and $P_{0.5\%}$ were reproduced with high accuracy during the focused wave tests (Figure 4.15). Regarding the uplift pressures, these seem to be underestimated during the focused wave attack. That could possibly be explained considering the different wave shape during the irregular sea state, but mostly the preceding wave, which in the case of the focused signal is absent, as a water level depression precedes the wave impact at the structure.
- **Pressure distribution:** The focused wave signal was found to reasonably well reproduce the pressure distribution at the vertical face of the crest wall but seemed to underestimate the uplift pressures in the base plate (Figure 4.17).
- **Integrated Forces:** Results showed that a focused wave was able to reproduce the integrated horizontal force acting on the vertical face of the structure with a 15% margin compared to the irregular sea state (Figures 4.18 and 4.19). However, it was observed that obtaining the same incident wave height at the toe does not necessarily imply that the total force or peak impact pressure will be identical. That is reasonable as the impact occurs under different conditions in terms of the preceding waves.

5.2. Recommendations

The aforementioned points indicate that using this type of compact wave signal, following the formulation of Tromans et al. (1991) for the characteristic shape of the extreme sea state, is promising as the wave impacts were able to reproduce the extreme hydraulic responses recorded from the reference tests of a thousand waves in an irregular sea state. Therefore, this study demonstrates the potential of using this type of wave signals to reproduce not only the maximum waves corresponding to an irregular sea state, but also the sliding failure in crest walls and the maximum impulsive loads. The early stage of this finding and limited test campaign comes short to sufficiently support these conclusions, and make this approach broadly applicable, however, show this method is promising and points the direction to future research towards the following points:

- Further investigate and define the full parameter space for the focused wave that is relevant for applying this wave theory (Tromans et al. 1991) for reproducing extreme hydraulic responses. For instance: focal point, phase at focus (e.g. trough or crest focused etc.), relevant range for the celerity enhancement factor. Also, investigate more spectral shapes, e.g., by means of a varying peak enhancement factor for the JONSWAP spectrum, and investigate also other types of spectra.
- Research how these compact, focused wave signals can be used as an integral part of larger test campaigns, as it is not clear if they can reproduce a complete statistical distribution of wave forces that is needed for the design of coastal structures. Along the same lines, identify in which parts of an experimental campaign of modelling a coastal structure these focused wave signals can be safely used to reduce testing times. For instance, after a full wave train is tested and the statistical distribution of pressures acting upon the structure are produced, then short wave signals that can reproduce peak pressures can be created, and the results of hydraulic response can be correlated to those of the irregular sea state in a sound, consistent manner. These short tests, lasting about one minute, could be used to reproduce extreme responses many times, instead of testing (a few) thousand waves to record perhaps just a couple of extreme pressures.

References

- Allsop, N. W. H., Vicinanza, D., & McKenna, J. E. (1996). Wave Forces on Vertical Composite Breakwaters, Report SR 443. HR Wallingford.
- Altomare, C., Gironella, X., Marzeddu, A., Recasens, M. V., Mosso, C., & Sospedra, J. (2024). Impact of focused wave groups on pier structures: a case study of severe breaking waves at Pont del Petroli during storm Gloria. **Front. Built Environ.**, Sec. Coastal and Offshore Engineering. https://doi.org/10.3389/fbuil.2024.1372906
- Altomare, C., Chen, X., Suzuki, T., Raby, A., & Gironella, X. (2024). Overtopping Flow Velocity Characterisation of Focused Waves on Promenades Using the Bubble Image Velocimetry Technique. **Coastlab**, Conference Proceedings. https://doi.org/10.59490/coastlab.2024.719
- Bagnold, R. A. (1939). Interim Report on Wave-Pressure Research.
- Battjes, J. A., & Bijker, E. W. (1969). **Research on Wave Action Symposium**, Conference Proceedings, Delft Hydraulics Laboratory, Delft, The Netherlands.
- Biésel, F. and Suquet, F. (1952). Laboratory Wave-generating Apparatus
- Chen, X., Hofland, B., Molenaar, W., Capel, A., van Gent, M. R. A. (2019). Use of impulses to determine the reaction force of a hydraulic structure with an overhang due to wave impact, **Coastal Engineering**, 147, 75-88.
- Cuomo, G., Allsop, N. W. H., Takahashi, S., & Kortenhaus, A. (2010). Breaking wave loads at vertical seawalls and breakwaters. **Coastal Engineering**, 57(4), 424-439.
- De Ridder, Kramer, J, den Bieman, J. P., Wenneker, I, (2023), Validation and practical application of nonlinear wave decomposition methods for irregular waves, **Coastal Engineering**, https://doi.org/10.1016/j.coastaleng.2023.104311.
- Frostick, L., McLelland, S. J., & Mercer, T. G., et al. (2011). Users guide to physical modelling and experimentation. **IAHR design manual.**
- Fuhrboter, A. (1969). Laboratory investigation of impact forces. **Research on Wave Action Symposium**, Conference Proceedings, Delft Hydraulics.
- Goda, Y. (2000). Random Seas and Design of Maritime Structures. **World Scientific.**
- Jacobsen, N. G., van Gent, M. R. A., Capel, A., & Borsboom, M. (2018). Numerical prediction of integrated wave loads on crest walls on top of rubble mound structures. **Coastal Engineering**. https://doi.org/10.1016/j.coastaleng.2018.10.
- Hofland, B., Kaminski, M., & Wolters, G. (2010). Large Scale Wave Impacts on a Vertical Wall. **Int. Conf. Coastal Eng.**, doi: 10.9753/icce.v32.structures.15.
- Hofland, B., Wenneker, I., & van Steeg, P. (2014). Short Test Durations for Wave Overtopping Experiments. **Coastlab**, Conference Proceedings.
- Holthuijsen, L. H. (2007). Waves in Oceanic and Coastal Waters. **Cambridge University Press.**

- Hughes, S. A. (1993). Physical Models and Laboratory Techniques in Coastal Engineering. **World Scientific Publishing.**
- Jensen, O. J. (1984). A Monograph on Rubble Mound Breakwaters.
- Lundgren, H. (1969). Wave Shock Forces: An Analysis of Deformations and Forces in the Foundation. **Research on Wave Action Symposium, Conference Proceedings**, Delft Hydraulics.
- Lykke Andersen, T., Røge Eldrup, M., Estimation of incident and reflected components in nonlinear regular waves over sloping foreshores, 2021, **Coastal Engineering,** https://doi.org/10.1016/j.coastaleng.2021.103974.
- Madsen, O (1970). Waves generated by a piston type wave maker, Coastal Engineering Research Centre, USACE.
- Mc Connel, K., J., and Koortenhaus, A., (1997) Analysis of pressure measurements from hydraulic model tests and prototype measurements Proc., PROVERBS project, Leichtweiss Institut, Technical University of Braunschweig, Braunschweig, Germany.
- Mortimer, M., Calvert, R., Antonini, A., Greaves, D., Raby, A., v.d. Bremer, T., (2023), Implications of second-order wave generation for physical modelling of force and run-up on a vertical wall using wave groups, Coastal Engineering, Volume 180, https://doi.org/10.1016/j.coastaleng.2022.104259.
- Pedersen, J., (1996) Wave forces and overtopping on crown walls of rubble mound breakwaters: an experimental study. PhD Thesis
- Saville, L. H. (1940). Presidential Address of Sir Leopold Halliday Saville, KCB, President 1940-1941. **ICE Journal**, Volume 15, Issue 1, pp. 1-26.
- Tromans, P. S., Anaturk, A. R., & Hagemeijer, P. (1991). A new model for the kinematics of large ocean waves - application as a design wave. In The First **International Offshore and Polar Engineering Conf.**, Edinburgh, Int. Soc. of Offshore and Polar Engs.
- Van Gent, M. R. A., & van der Werf, I. M. (2019). Influence of oblique wave attack on wave overtopping and forces on rubble mound breakwater crest walls. **Coastal Engineering**. https://doi.org/10.1016/j.coastaleng.2019.04.001.
- Weigel, R. L. (1964). **Oceanographical Engineering**. Prentice-Hall, New Jersey.
- Whittaker, C. N., Fitzgerald, C. J., Raby, A. C., Taylor, P. H., & Borthwick, A. G. L. (2018). Extreme coastal responses using focused wave groups: Overtopping and horizontal forces exerted on an inclined seawall. **Coastal Engineering**. https://doi.org/10.1016/j.coastaleng.2018.08.004.
- Whittaker, C. N., Fitzgerald, C. J., Raby, A. C., Taylor, P. H., Orszaghova, J., & Borthwick, A. G. L. (2017). Optimisation of focused wave group runup on a plane beach. **Coastal Engineering**. https://doi.org/10.1016/j.coastaleng.2016.12.001.
- Zelt J.A., and Skjelbreia J. E., (1992) Estimating Incident and Reflected Wave Fields Using an Arbitrary Number of Wave Gauges, **Int. Conf. Coastal Eng.**, https://doi.org/10.1061/9780872629332.058

List of Figures

List of Tables

Acknowledgements

This research project offered me a joyful journey of research, especially when re-discovering from my experiments findings of research studies carried out in the past decades – but none of these things would have happened without the following contributions. First and foremost, I would like to thank the main supervisor of this work, dr. ir. Bas Hofland, for supporting this idea, his guidance, help and enthusiasm along the way, his detailed review and comments that significantly improved the quality of this report, and the opportunity to gain some first experience in the exciting world of physical modelling. I would like to thank the co-supervisor from TU Delft, dr. ir. Alessandro Antonini for accepting to supervise this work and his enthusiasm about the topic. Special thanks to Darryl de Vos for providing his experimental set up to conduct the experiments of this study, for kindly providing the data of the irregular wave tests and the nice collaborative work in the lab. I must also thank Jeniffer Rodriguez from the HE Lab for the information regarding the wave machine required to formulate the custom steering signals. I would like to thank Prof. Marcel van Gent for our brief discussion about impact forces whilst I was conducting the experimental campaign for my thesis in Deltares, which prompted me to have a more careful look into the dataset of pressures and to include integrated forces in the analysis. Lastly, many thanks to my family for their continuous support, and to my partner for brightening up my days.

Appendix

A. Experimental Set up

A.1. Testing Section

Figure A1.1. Testing Section in the laboratory flume.

A.2 Pressure sensors deployment

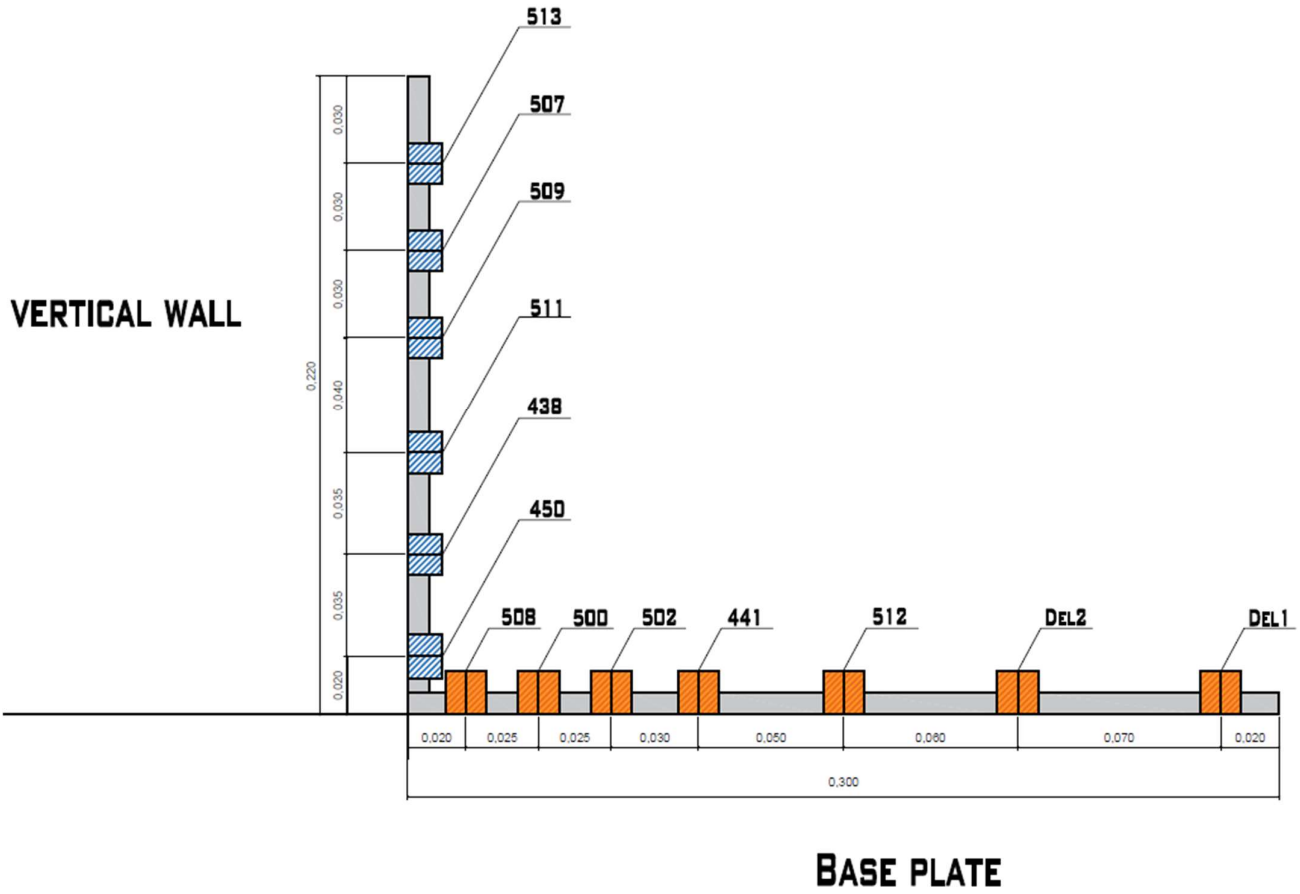

Figure A2.1. Deployment of pressure sensors at the vertical face and the base plate of the crest wall. The crest wall has a total height of 0.22 m and a width of 0.30 m. In the base plate of the crest wall seven pressure gauges are embedded in the plywood model crest wall. The base plate of the crest wall lays directly on the core of the breakwater. A splashboard was placed above the model crest wall during the experiments to avoid interference of the measurement by the water volumes that overtopped.

B. Test Results

5.3. B1. Calibration runs

Table B1.1 Tests Series A and B

Test ID	Focal point from wave paddle [m]	Input spectral wave height H [m]	Input spectral wave period Tp [s]	Note
Test A000 (1-3)	30.47	0.15	2.53	Gain factors: 0.5, 0.8, 1.
Test A001 (1-3)	30.47	0.17	2.53	Gain factors: 0.5, 0.8, 1.
Test B000 (1-2)	32.87	0.15	2.53	Gain factors: 0.8 and 1.
Test B001	37.87	0.15	2.53	Gain factor: 0.8
Test B002	34.34	0.15	2.53	Gain factors: 0.8

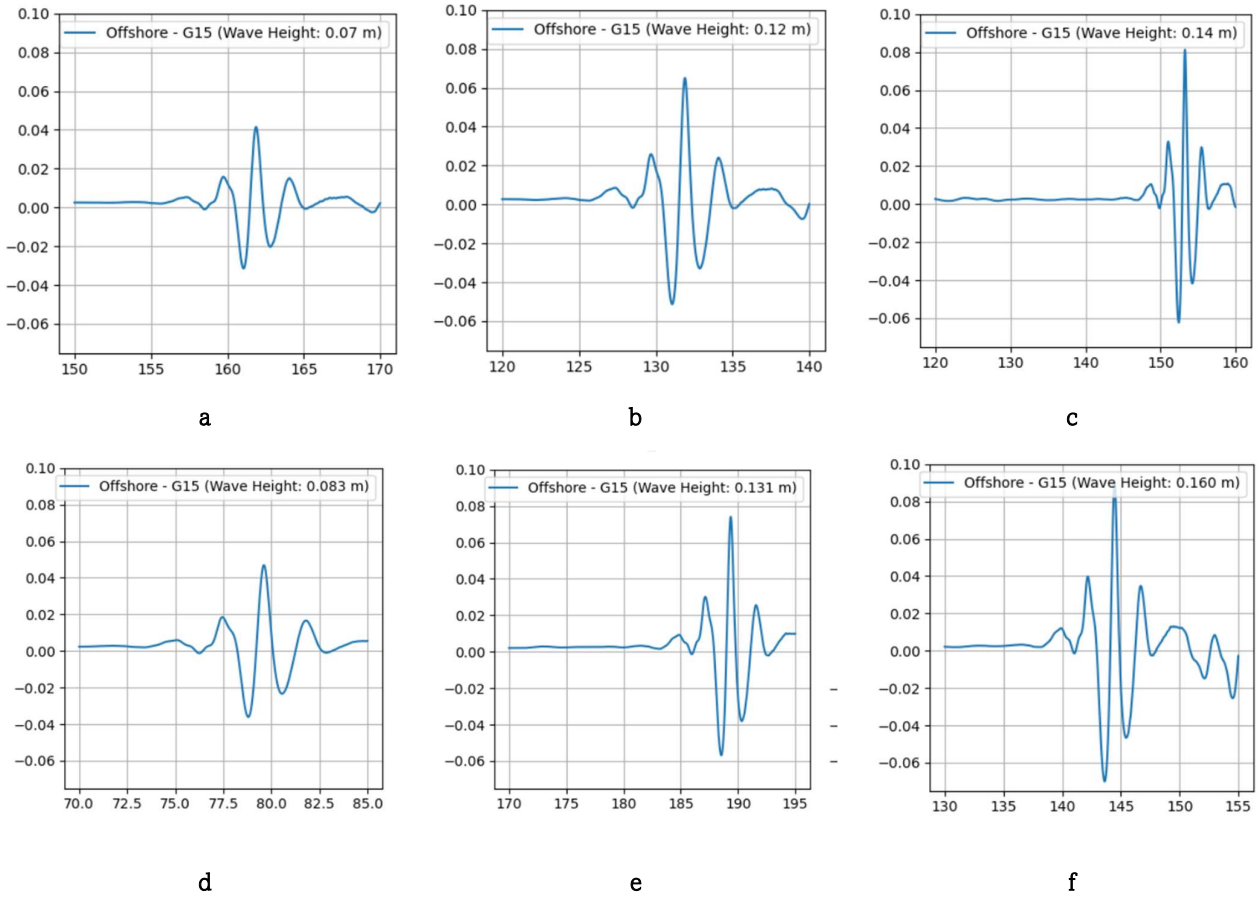

Figure B1.1 Free surface elevation for test series A, recorded at wave gauge G15, located offshore (away from the structure). a) Test A000-05 b) Test A000-08 c) Test A000-1 d) Test A001-05 e) Test A001-08 f) Test A001-1. Tests A000-1 to A000-3 have the same input spectral parameters Hs = 0.15 m and Tp = 2.53 s with varying gain factors 0.5, 0.8 and 1. Tests A001-1 to A001-3 have the same input spectral parameters Hs = 0.17 m and Tp = 2.53 s with

varying gain factors 0.5, 0.8 and 1. Focal distance is set to 30.47 m for all tests, and gauge 15 is located, 24.5 m from paddle rest position.

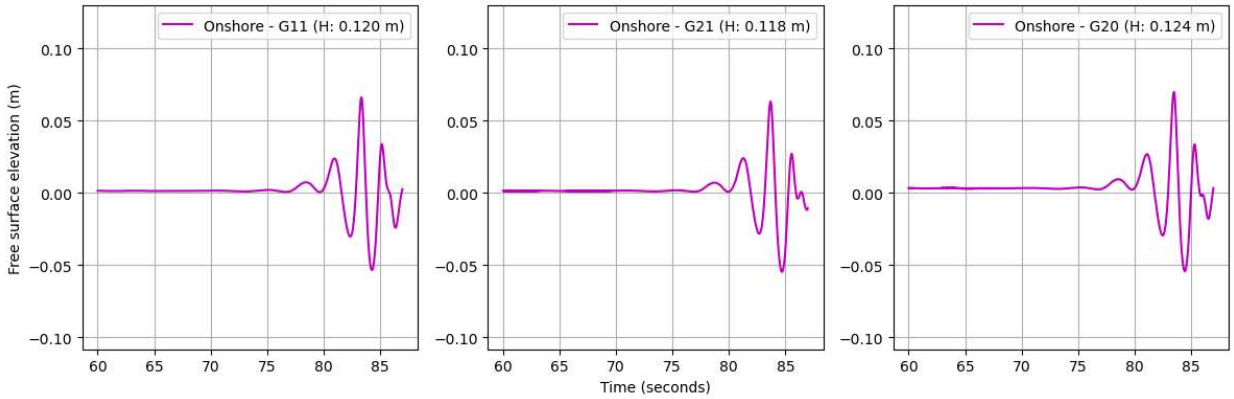

Figure B1.1 Test B00, Focal point xf =32.87 m, gain factor = 0.8.

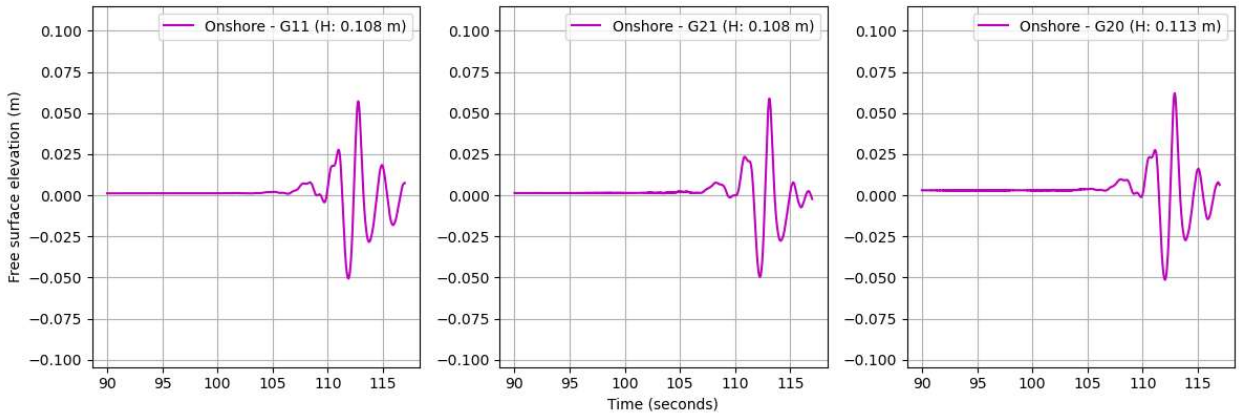

Figure B1.2 Test B01, Focal point xf =37.87 m, gain factor= 0.8.

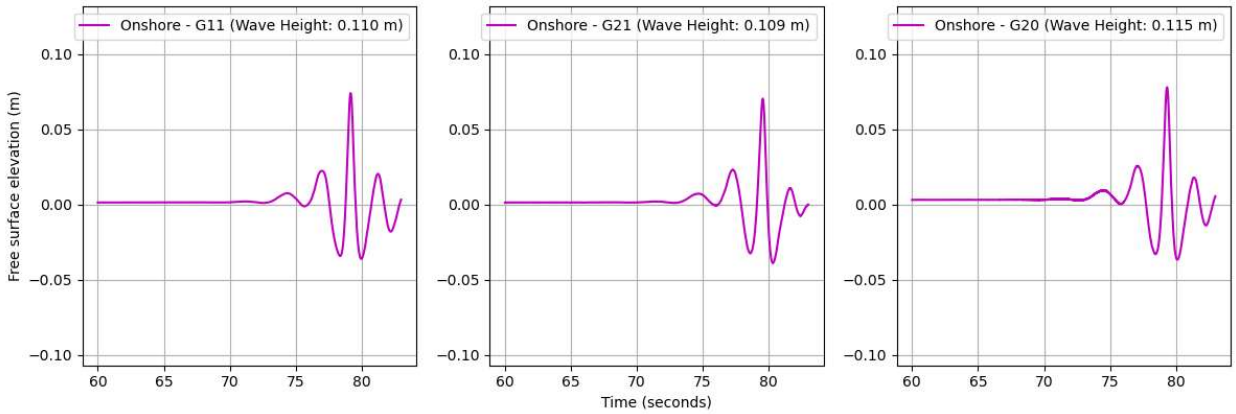

Figure B1.3 Test B002, Focal point xf = 34.34 m, gain factor= 0.8.

B2. Results Test Series E

Table B2.1 Test Series E, test programme and recorded wave heights at the offshore measurement location, wave gauge G15.

#	Test ID	Focal distance from the paddle	Incident wave height, recorded at gauge G15
1	1204_E000	x_f = 29.00 m	H = 0.2412 m
2	1204_E001	x_f = 24.00 m	H = 0.2327 m
3	1204_E002	x_f = 24.10 m	H = 0.2335 m
4	1204_E003	x_f = 24.20 m	H = 0.2332 m
5	1204_E004	x_f = 24.70 m	H = 0.2367 m
6	1204_E005	x_f = 25.20 m	H = 0.240 m
7	1204_E006	x_f = 25.70 m	H = 0.245 m
8	1204_E007	x_f = 26.70 m	H = 0.238 m
9	1204_E008	x_f = 27.23 m	H = 0.252 m
10	1204_E009	x_f = 27.33 m	H = 0.253 m
11	1204_E010	x_f = 27.43 m	H = 0.254 m

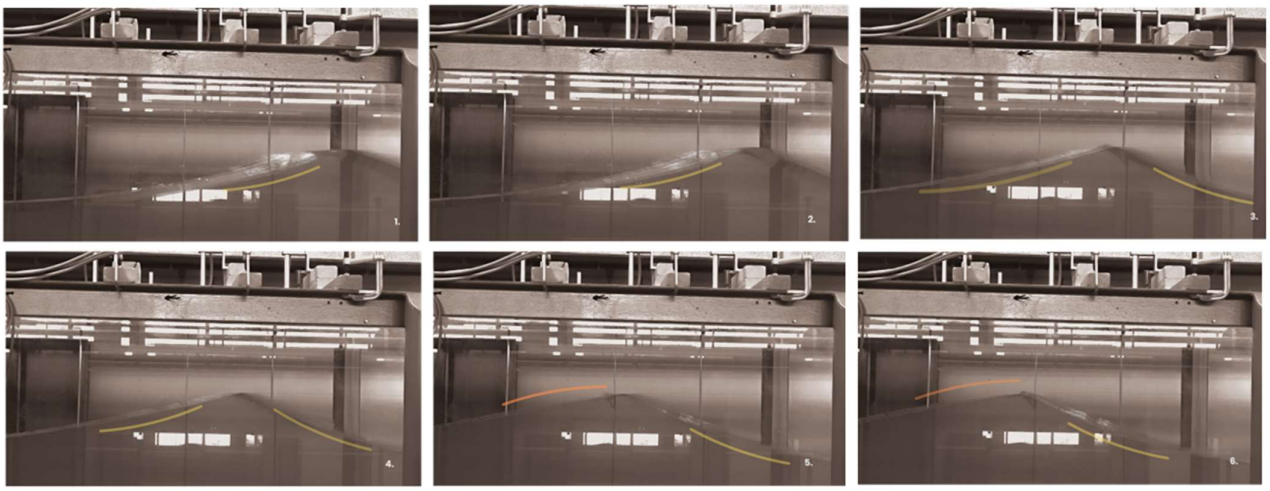

Figure B2.1. Photos of the free surface elevation for test E010 as the wave propagates at the most offshore gauge triplet. Recorded incident wave height, Hi = 0.254 at gauge 15. Yellow lines in panels 1-3 indicate the convex shape of the water surface surrounding the peak, while, at panels 5 and 6 the shape of the preceding front becomes concave. Results of the measured wave heights indicate that this shape occurs post-focus, where the measured wave height starts to decay, whereas until the focal point, the wave height gradually increases.

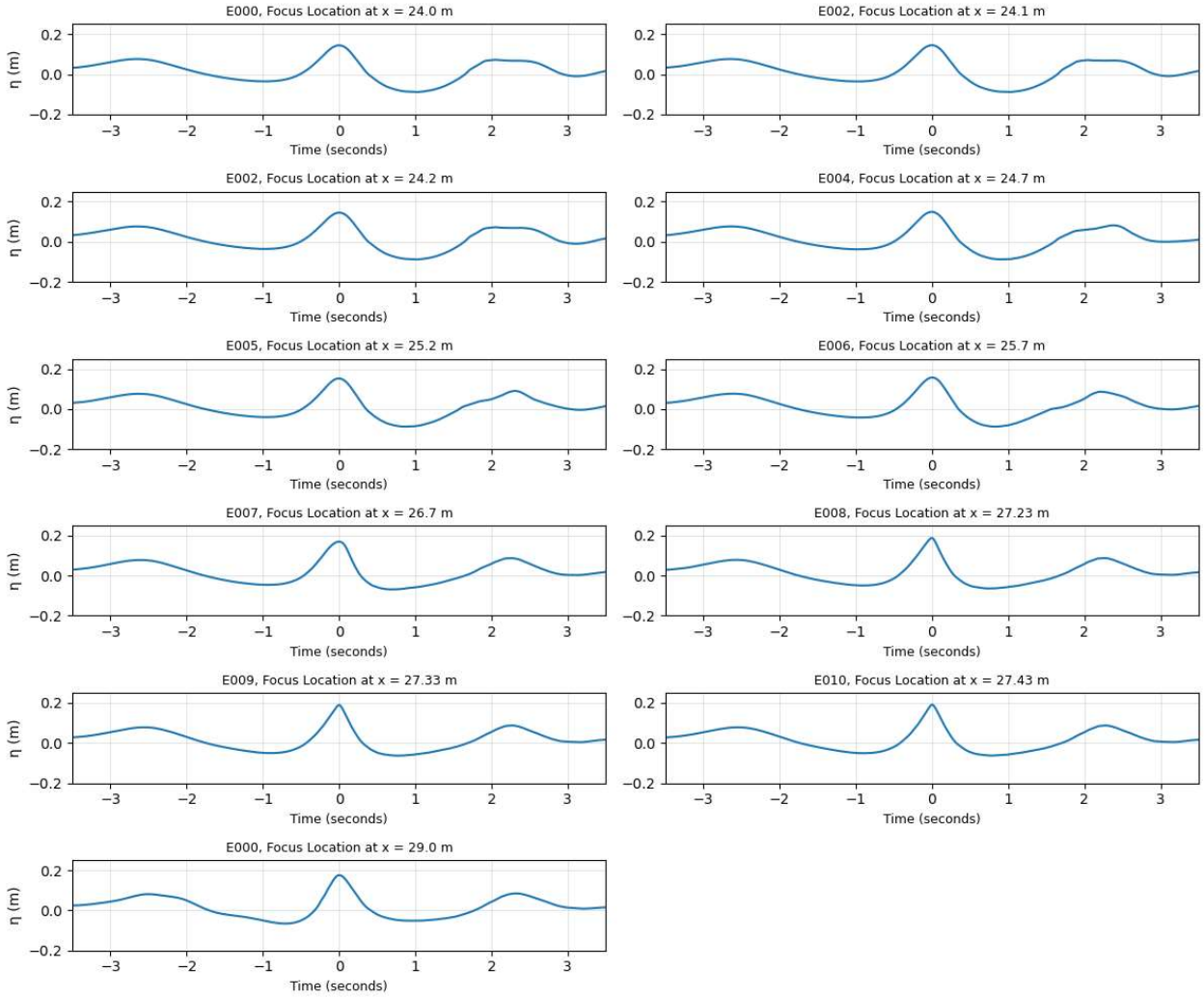

Figure B2.2 Free Surface elevation for all tests of Test Series E, measured at gauge, G15. The steered wave signal differs only with respect to target focal distance which varied between 24.0 m and 29.0 defined from the resting position of the wave-maker.

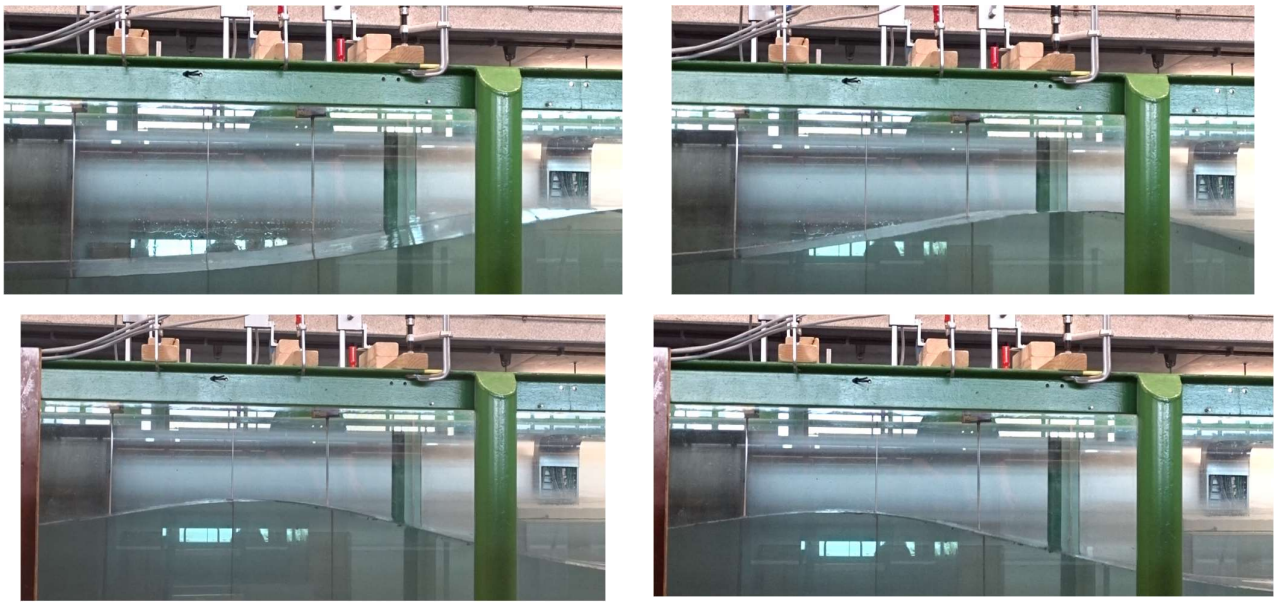

Figure B2.3. Photo sequence from focused wave test E004 at the offshore measurement location, target focal point, xf = 24.7 m, incident wave height, hi = 0.237 m measured at gauge G15.

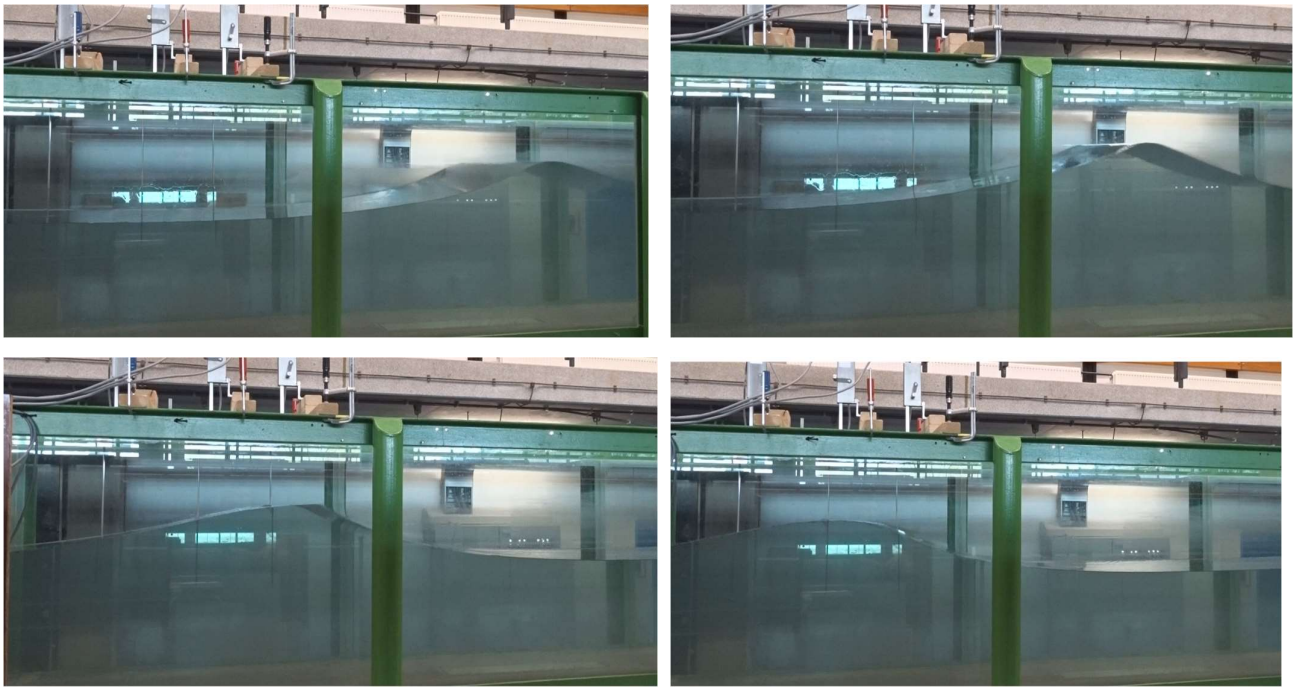

Figure B2.4 Photos during focused wave test E007 at the offshore measurement location, target focal point: xf =26.70 m, incident wave height, Hi = 0.238 m measured at gauge G15.

B3. Impact Tests

All tests of group C – Impact tests, were simulated with, peak period Tp = 2.53 s and water level so that the crest wall is emergent with foundation level Fc = + 0.03 m from still water level. Test series D, include steeper waves, corresponding to $s_{o,p}$= 4% in the irregular sea state, with Tp= 1.55 s.

Table B2.1 Test Series C, overview of test programme.

#	Test	Celerity enhancement factor, alpha	Focus point [m]	POT
1	1104_C000	1.06	32.9	0.6
2	1104_C001_1	1.06	32.9	0.8
3	1104_C001_2	1.06	32.9	1.
4	1104_C002_1	1.06	30.5	0.8
5	1104_C002_2	1.06	30.5	1.
6	1104_C003_1	1.06	32.5	0.7
7	1104_C003_2	1.06	32.5	0.8
8	1104_C003_3	1.06	32.5	0.9
9	1104_C003_4	1.06	32.5	1
10	1104_C004_1	1.04	32.5	1
11	1104_C005_1	1.02	32.5	1
12	1104_C006_1	1	32.5	0.8
13	1104_C006_2	1	32.5	1

Table B2.2 Test Series D, overview of test programme.

#	Test	Foundation level, Fc (m)	Tp (s)	alpha	Focus point [m]	POT
1	1204_D000	0.03	1.55	1.06	32.5	0.8
2	1204_D001	0.03	1.55	1.06	32.5	1
3	1204_D002	0.03	1.55	1.06	32.5	0.9
4	1204_DCWL_1	0.01	1.55	1.06	32.5	1
5	1204_DCWL_2	0.01	1.55	1.06	32.5	0.9
6	1204_DCWL_3	0.01	1.55	1.06	32.5	0.8

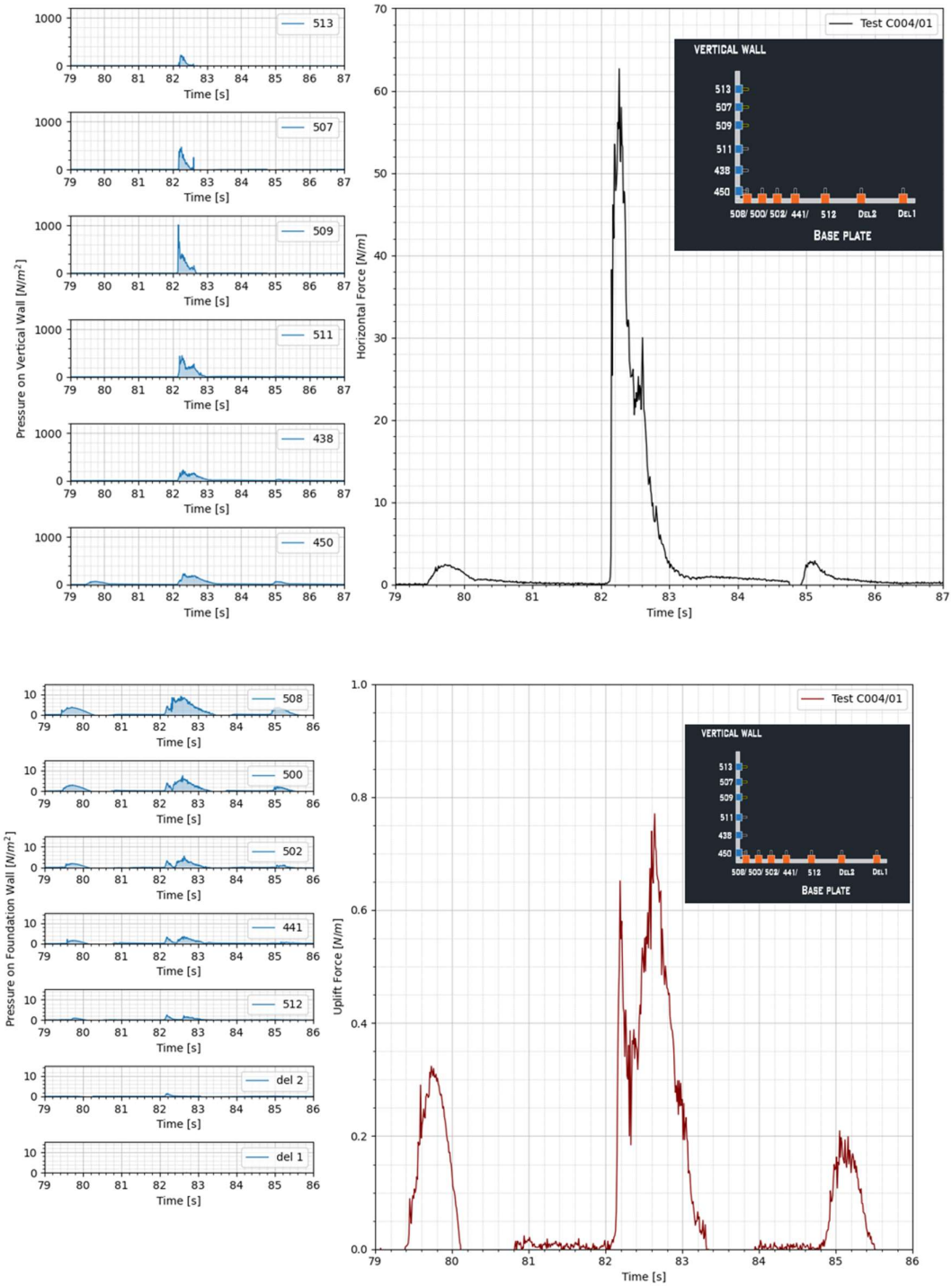

Figure B3.1. Pressure records and integrated forces on the vertical face and the base plate of the crest wall for focused wave test C004/1, incident wave height at the toe: Hi = 0.32 m, corresponding to 1:10000 waves.

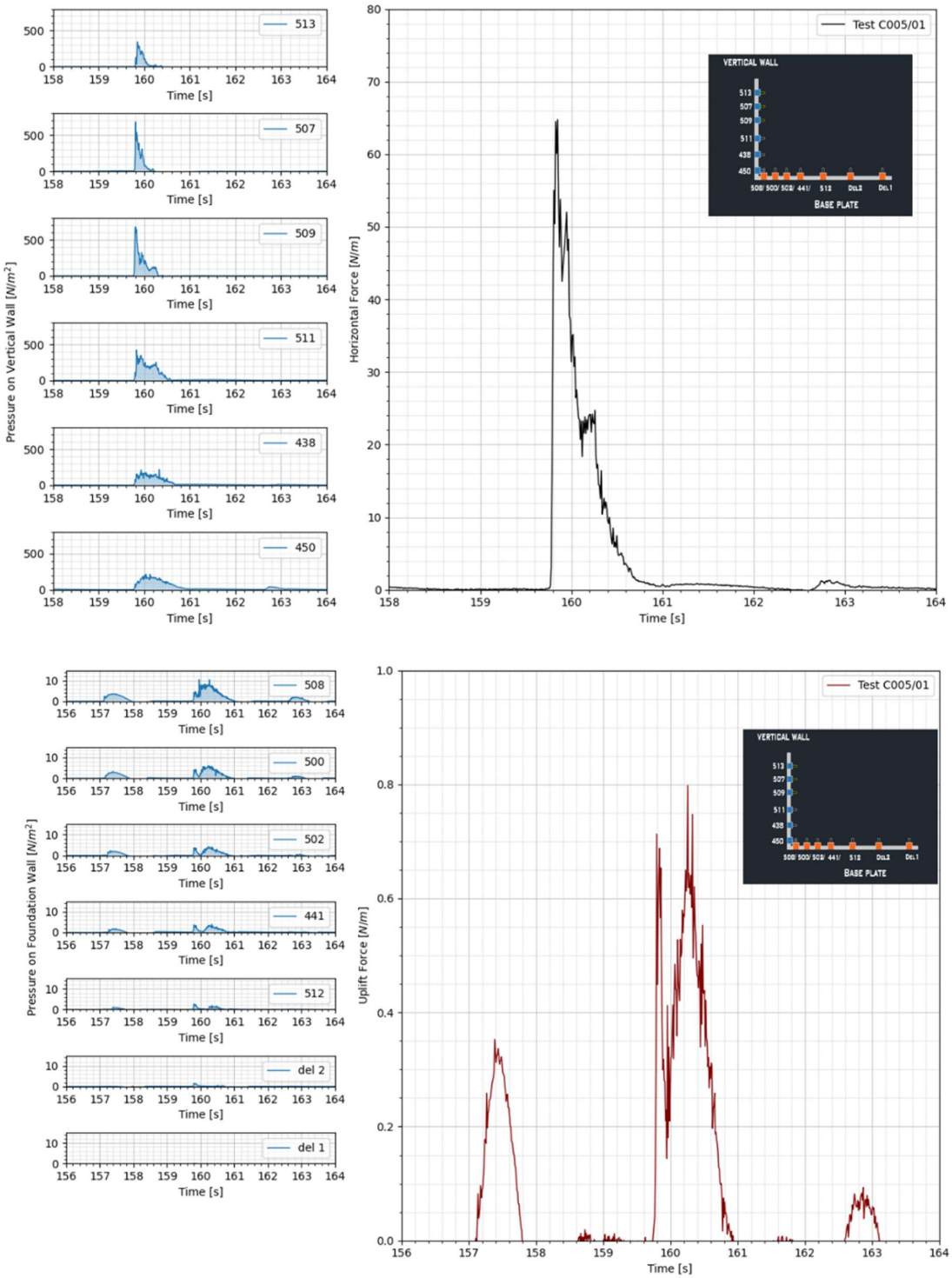

Figure B3.2. Pressure records and integrated forces on the vertical face and the base plate of the crest wall for focused wave test C005/1, incident wave height at the toe: Hi = 0.28 m, corresponding to 1:1000 waves.

C. Irregular Wave trains

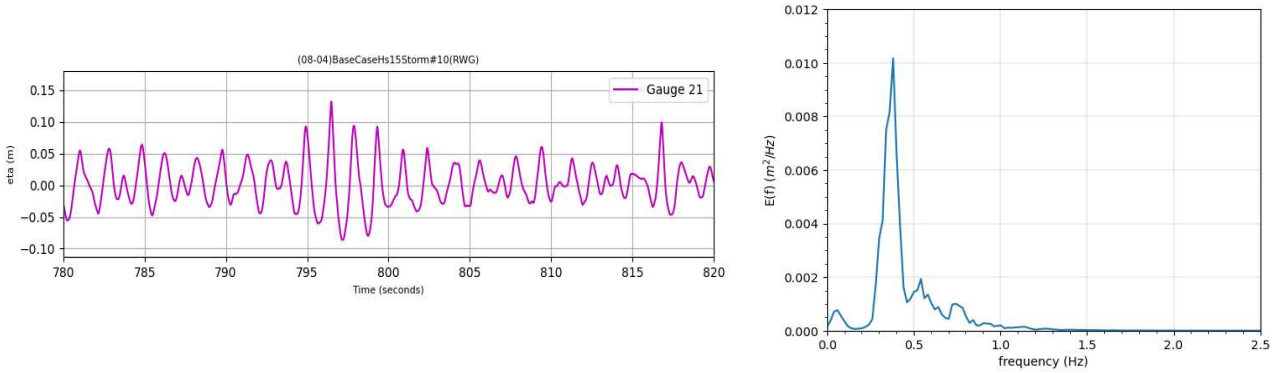

Figure **C1.** Snippet of free surface elevation timeseries from the irregular wave tests (left panel) and wave energy spectrum (right panel), of the full signal of irregular wave test of about a thousand waves, measured at Gauge 21, located about 2.3 m seaward of the toe of the structure.

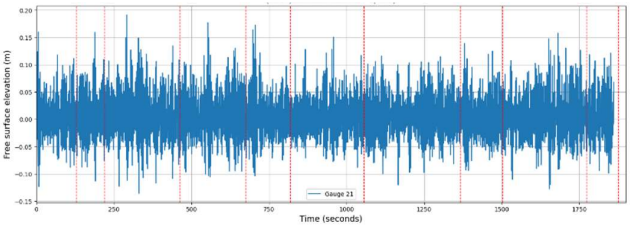

Figure C2. Irregular wave timeseries. Red lines indicate the times when peak pressures are tracked form the block maxima.

Table C1. Spectral and temporal wave parameters of irregular sea state.

Maximum Measured Wave Height, H_{max}	0.277 m
Significant Wave Height, H_s	0.149 m
Mean Zero Crossing Period, T_{mean}	2.040 s
Spectral Wave height, H_{m0}	0.155 m
Peak Wave Period, T_p	2.543 s
Spectral Wave Period, $T_{m-1,0}$	3.010 s
Spectral Mean, zero crossing period, $T_{m0,2}$	2.002 s

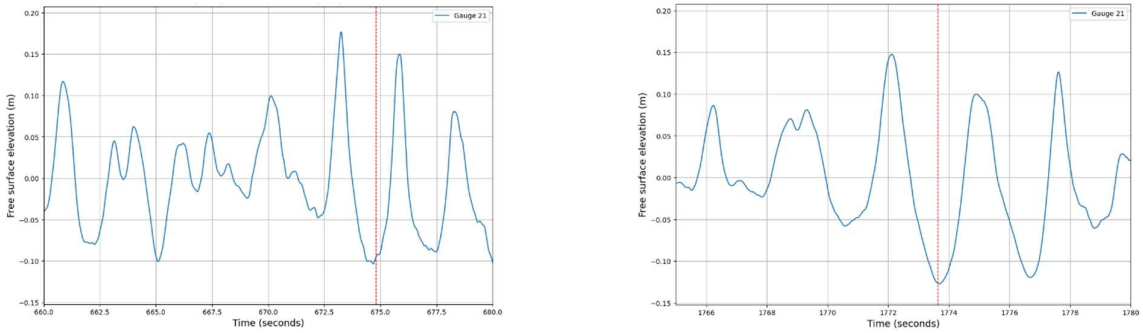

Figure C3. Wave records (total signal) of irregular sea state, target wave parameters Hs = 0.15 m, and Tp = 2.53 s. red lines indicate the time when the peak pressures are recorded from the bloc maxima, then used for comparison to pressures induced during the focused wave attack.